Geoscience Frontiers 14 (2023) 101483

Contents lists available at ScienceDirect

Geoscience Frontiers

journal homepage: www.elsevier.com/locate/gsf

Research Paper

Indian monsoon variability in the Mahanadi Basin over the last two glacial cycles and its implications on the Indonesian throughflow

Jongmin Lee [a,b], Sunghan Kim [c], Minoru Ikehara [d], Keiji Horikawa [e], Yoshihiro Asahara [f], Chan Min Yoo [b], Boo-Keun Khim [a,*]

[a] Department of Oceanography, Pusan National University, Busan 46241, South Korea
[b] Deep-sea Mineral Resources Research Center, Korea Institute of Ocean Science & Technology, Busan 49111, South Korea
[c] Division of Glacial Environment Research, Korea Polar Research Institute, Incheon 21990, South Korea
[d] Center for Advanced Marine Research, Kochi University, Kochi 783-8502, Japan
[e] Graduate School of Science and Engineering for Research, University of Toyama, Toyama 930-8555, Japan
[f] Department of Earth and Planetary Sciences, Nagoya University, Nagoya 464-8601, Japan

ARTICLE INFO

Article history:
Received 5 March 2022
Revised 16 August 2022
Accepted 23 September 2022
Available online 29 September 2022
Handling Editor: E. Shaji

Keywords:
Provenance
Weathering activity
Paleo-productivity
Indian summer monsoon
Bay of Bengal
Indonesian throughflow

ABSTRACT

The orbital-scale variability of the Indian summer monsoon (ISM) has been influenced by multiple factors, such as atmospheric CO_2 concentration, global ice volume, and insolation. Proxies for weathering activity and paleo-productivity provide potential insights into the driving forces of its variability. We documented multi-proxy data at IODP Site U1445, located in the Mahanadi Basin of the northwestern Bay of Bengal, to find out ISM variability over the last 200 ka. The proxy records, such as Nd/Sr isotopes of detrital particles, clay mineral compositions of the fine-grained sediments, biogenic opal and $CaCO_3$, organic carbon contents, and carbon isotopes of organic matter, represent sediment sources, weathering patterns, and paleo-productivity related to the ISM variability. Detrital Nd/Sr isotope data and clay mineral compositions suggest that the sediments at Site U1445 originated mainly from the Ganges, Brahmaputra, and Meghna rivers without dramatic provenance change between the glacial and interglacial periods. The weathering activity inferred from clay mineral compositions and the paleo-productivity shift reconstructed by biogenic opal and $CaCO_3$ contents suggest that the land-sea interactions were closely linked to the ISM precipitation between the glacial and interglacial periods. High precipitation by the strong ISM resulted in intense chemical weathering and dominant biogenic opal deposition during the interglacial periods. In contrast, low precipitation by the weak ISM led to reduced chemical weathering and predominant $CaCO_3$ deposition during the glacial periods. Further, the ISM variability driving the land-sea interactions in the Mahanadi Basin was modulated by the Indonesian throughflow (ITF). Our study emphasizes the role of low-latitude forcing of climatic changes in the strong relationship between the ISM and ITF over orbital periods, providing a base for future investigations.

1. Introduction

The Indian monsoon, one of the Asian monsoon systems, is driven by the seasonal reversal of temperature gradients between the continent and the ocean (Wang et al., 2017). Warm and humid airs are transported toward the Indian subcontinent from the tropical ocean during the summer, resulting in high precipitation in the Himalayan and nearby regions. The Indian monsoon has evolved alongside regional and global climate change (e.g., Chang et al., 2018). Various paleoclimate records have been used to reconstruct the historical variability in the Indian monsoon to help understand future hydrological change and related land-sea interaction. According to proxy reconstructions and modeling studies, the Indian monsoon variability was affected by diverse factors such as orbital forcing, global ice volume, ocean gateway, and orogeny (i.e., Himalayan-Tibetan Plateau uplift), which are mainly generated by the high-latitude forcing on different geological timescales (Thomson et al., 2021). For instance, a gradually increasing trend of dry conditions in the southern Asian regions was reported as a result of the weakening of Indian summer monsoon (ISM) strength related to global cooling since the late Miocene (Huang et al., 2007; Clift et al., 2008; Lee et al., 2020a). On shorter timescale, ISM

* Corresponding author.
E-mail address: bkkhim@pusan.ac.kr (B.-K. Khim).

https://doi.org/10.1016/j.gsf.2022.101483

rainfall was reduced during Heinrich events of the North Atlantic realm at millennial timescales (Colin et al., 1998).

The Quaternary is a remarkable period characterized by distinct interglacial-glacial cycles related to the growth and decay of continental ice sheets in the Northern Hemisphere (Lisiecki and Raymo, 2007). Many studies on weathering intensity (Lupker et al., 2013; Ota et al., 2018; Yu et al., 2020; Liu et al., 2020), sedimentary processes (Panmei et al., 2018; Li et al., 2019), paleo-productivity regimes (Devendra et al., 2019; Ota et al., 2019), and vegetation compositions (Zorzi et al., 2015; Contreras-Rosales et al., 2014) have emphasized that the global ice volume has been a key high-latitude forcing that modulates the Indian monsoon variability between the interglacial and glacial periods. However, Saraswat et al. (2019) reported that warming in the equatorial Indian Ocean during interglacial periods results in heavy Indian monsoon precipitation, and *vice versa* during the glacial periods. From this implication, the potential roles of the sea surface temperature (SST) in the equatorial Indian Ocean on the variability of ISM rainfall during the interglacial-glacial cycles have been proposed as low-latitude forcing (Saraswat et al., 2019; Pang et al., 2021).

Recently, Jin and Wright (2020) reported that SST variations in the equatorial Indian Ocean are significantly affected by the Indonesian throughflow (ITF), which is the main surface current exchanging seawater between the Pacific and Indian Oceans (Fig. 1a; Gordon, 2005). Some studies have already highlighted the importance of the ITF as a controlling force related to climatic changes, because the substantial heat and moisture transported by the ITF influence hydrological variability in the low-latitude tropical ocean (e.g., Sprintall and Rèvelard, 2014). In this context, several studies suggested that hydrological climate change in the Asian continent (i.e., Asian monsoon systems) was sensitive to ITF variability at the tectonic and orbital timescales (Petrick et al., 2019; Saraswat et al., 2019; Su et al., 2019; Pang et al., 2021). For example, Su et al. (2019) suggested that the drying in the central Asia region is synchronous with the opening timing of the Indonesian Seaway, resulting in a weakening of the ITF.

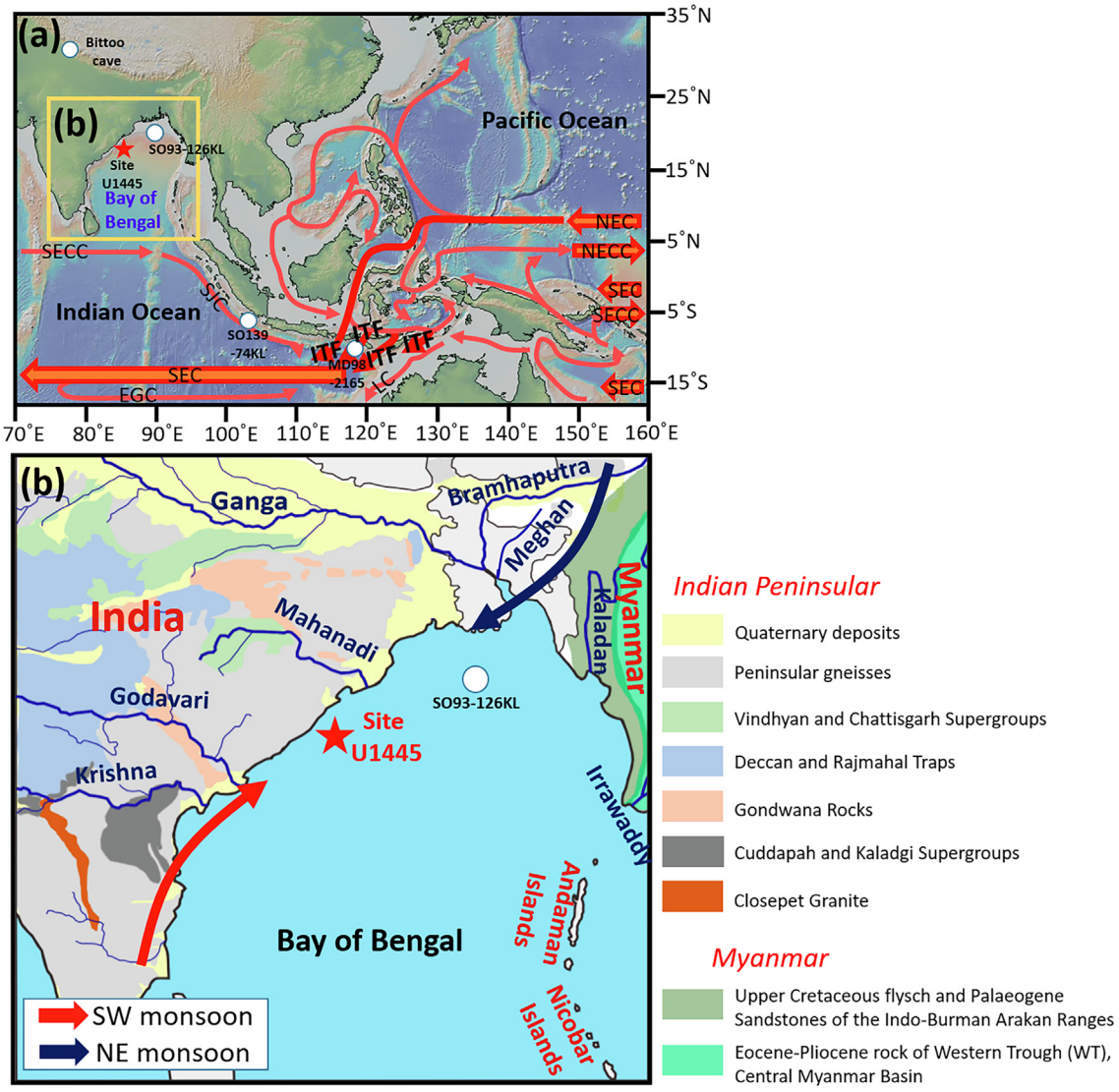

Fig. 1. (a) Overview of oceanic surface currents (NEC: North Pacific Equatorial Current, NECC: North Equatorial Counter Current, *SEC*: South Equatorial Current, SECC: South Equatorial Counter Current, LC: Leeuwin Current, SJC: South Java Current, EGC: East Gyral Current, ITF: Indonesian throughflow) and the locations of Site U1445 (red star) and other sites (white circles) used in this study (SO139-74KL and MD98-2165 (Pang et al., 2021), SO93-126KL (Kundrass et al., 2001), and Bittoo Cave (Kathayat et al., 2016)). (b) Map of the Bay of Bengal showing the locations of Site U1445 and SO93-126KL, lithology of river drainage basins with the major rivers (Ganges, Bramhaputra, Meghan, Mahanadi, Godavari, Krishna, Kaladan, and Irrawaddy) in the Peninsular India and Myanmar region. Red (summer) and blue (winter) arrows represent the seasonal monsoon winds (For interpretation of the references to color in this figure legend, the reader is referred to the web version of this article).

Pang et al. (2021) examined the changes in the thermocline water temperature (TWT) record, which represents the relative strength of the ITF; the ITF was found to be stronger during the interglacial periods, which might have influenced the strength of the Indian monsoon. However, the limited SST and TWT records available for the equatorial Indian Ocean are insufficient to adequately substantiate an association between ITF changes and Indian monsoon variability. Further, these distal records cannot effectively capture the major and minor changes in Indian monsoon rainfall, which highly impact on river discharge and land dryness between the interglacial and glacial periods. Therefore, new integrated results with sufficient spatiotemporal records that have been reliably assessed are needed to improve our understanding of the relationship between ITF changes and ISM variability during the interglacial-glacial cycles.

In this study, we discussed the land-sea interactions in the Bay of Bengal (BOB) in response to the Indian monsoon variability at the orbital timescale over the past 200 kyrs. The analyses were based on multi-proxy sediment records (Nd and Sr isotopes, clay mineral compositions, biogenic opal and $CaCO_3$, organic carbon, and carbon isotope of organic matter) at International Ocean Discovery Program (IODP) Site U1445, located in the Mahanadi Basin of the northwestern BOB (Fig. 1a and b). These sediment records represent sediment source, weathering pattern, and surface water marine productivity. Further, our results regarding the land-sea interactions in response to the Indian monsoon variability can help better understand the linkage between the ISM and ITF in terms of low-latitude forcing of climatic changes.

2. Study area

2.1. Geologic and oceanographic settings of the Bay of Bengal

The BOB, which is strongly influenced by the Indian monsoon climate, is surrounded by Peninsular India, Myanmar, and the Andaman and Nicobar Islands (Fig. 1b). The Indian monsoon causes seasonal wind patterns and surface water circulation: cyclonic surface current is dominant by southwesterly wind in summer monsoon (SW monsoon) and anti-cyclonic surface current is dominant by northeasterly wind in winter monsoon (NE monsoon) (Schott and McCreary, 2001). It also causes seasonal precipitation variation, affecting runoff and terrigenous sediment input to the BOB (Webster, 1987). In particular, the flux of freshwater discharge in the Ganges-Brahmaputra-Meghan (GBM) river systems highly depends on the ISM rainfall, and the contribution of glacier melting water from Himalayan mountain is relatively weak (less than 25 % of stream flow) (Chowdhury and Ward, 2004). During the summer monsoon (SW monsoon), the BOB receives>90 % of its annual supply of freshwater (10×10^{12} m^3) and terrigenous sediment (15×10^6 metric tons) through the GBM river systems of the Himalayas in northern India and the Mahanadi, Godavari, and Krishna rivers in eastern India (Milliman and Farnsworth, 2011). The massive freshwater discharge derived from the major rivers results in strong water column stratification in the northern BOB (Narvekar and Kumar, 2014). Because the strong stratification during summer could overwhelm the offshore Ekman transport, the upwelling along the western margin of the BOB is limited, compared to the western Arabian Sea, despite the upwelling-favorable SW monsoon (Prasanna Kumar et al., 2002).

Prasanna Kumar et al. (2002) reported that the river systems of Peninsular India, including the GBM rivers, are the primary source of dissolved silicate in the BOB. Sarma et al. (2016) also observed that silicate concentration was generally higher in the low saline waters of the northern BOB, suggesting that freshwater flux from river systems is the principal controlling factor to supply silicate to the BOB. It has been reported that deep water below the mixed layer is the primary source supplying nitrate to the surface of the BOB (Singh et al., 2012). In the northern BOB, stratification caused by increased river discharge interrupts nitrate supply into the euphotic zone (Madhupratap et al., 2003). Miranda et al. (2020) also observed that nitrate concentrations were highest during weak precipitation and lowest during strong precipitation seasons in northwestern BOB. Despite the ample supply of nutrients from the river systems, primary productivity in the surface waters decreased during the summer, especially in northern BOB, because suspended particles caused a reduction in sunlight, and *vice versa* during the winter (e.g., Gomes et al., 2000).

2.2. Potential sediment sources to the Bay of Bengal

The GBM and Mahanadi, Godavari, and Krishna rivers transport terrigenous sediments from source regions to the BOB (Milliman and Farnsworth, 2011; Fig. 1b). In addition, the Irrawaddy river and other small rivers (e.g., Kaladan river) of the Indo-Burman-Arakan (IBA) Ranges in Myanmar cover the source regions of the terrigenous sediments to the eastern BOB and the Andaman Sea (Colin et al., 1999; Joussain et al., 2016; Miriyala et al., 2017). Due to the different lithologies in the drainage basins of these rivers, the terrigenous sediments originating from the different source regions are distinguished by the radiogenic Nd and Sr isotopes of detrital particles (Colin et al., 1999; Singh and France-Lanord, 2002; Singh et al., 2008; Ahmad et al., 2009; Licht et al., 2013; Lupker et al., 2013; Joussain et al., 2016; Awasthi et al., 2018; Giosan et al., 2018; Lee et al., 2020a; Peketi et al., 2021).

The detrital particles derived from the Ganges (ε_{Nd} values: −21.3 to −16.5 and $^{87}Sr/^{86}Sr$ ratios: 0.758 to 0.802), Brahmaputra (-19.0 to −12.5 and 0.719 to 0.755), and Meghna (-17.0 to −13.7 and 0.723 to 0.746) rivers are characterized by the distinctly different ε_{Nd} values and $^{87}Sr/^{86}Sr$ ratios (Singh and France-Lanord, 2002; Lupker et al., 2013; Awasthi et al., 2018). Previous study reported that the integrated GBM river systems were the most significantly contributor of sediments to the BOB during the past several million years (Awasthi et al., 2020). In addition, Kida and Yamazaki (2020) reported that about 85 % of riverine water entered the BOB through the main stream of integrated the GBM river systems. This means the GBM river systems can be used as the main source to sediment provenance in the BOB. For example, Lupker et al. (2013) already showed that the Nd and Sr isotopic compositions of marine sediments in the northern part of the BOB are similar to those of the GBM river systems and remained roughly constant (ε_{Nd} values: −16.1 to −15.4 and $^{87}Sr/^{86}Sr$ ratios: 0.734 to 0.743) without significant change over the last 21 kyrs. Ahmad et al. (2009) reported the isotope data of sediments in the Godavari (ε_{Nd} values: −18.2 to −15.3 and $^{87}Sr/^{86}Sr$ ratios: 0.720 to 0.730) and Krishna (ε_{Nd} values: −12.8 to −12.0 and $^{87}Sr/^{86}Sr$ ratios: 0.721 to 0.730) rivers. Recently, Peketi et al. (2021) measured the $^{87}Sr/^{86}Sr$ ratio (from 0.753 to 0.781) and ε_{Nd} values (from –22.2 to −19.2) of bed load sediments in the Mahanadi river. The Irrawaddy river sediments are characterized by different ε_{Nd} values (-7.3 to −6.8) and $^{87}Sr/^{86}Sr$ ratios (0.711 to 0.712) (Giosan et al., 2018). The Nd and Sr isotopic compositions of the IBA Ranges vary from −8.9 to −2.0 and from 0.702 to 0.710, respectively (Colin et al., 1999; Awasthi et al., 2014; Miriyala et al., 2017).

Similar to Nd-Sr isotope systematics, the spatial distribution of clay minerals in the surface sediments of the BOB has also been studied to track the primary provenance of fine-grained particles (Phillips et al., 2014; Joussain et al., 2016; Li et al., 2017, 2018; Sun et al., 2020). In the northern and central parts of the BOB, illite content is high (48 % to 78 %), which reflects that the fine-grained sediments were derived mainly from the GBM rivers (Li et al., 2017, 2018). Mixing of sediments derived from the rivers in Penin-

sular India, including the Mahanadi, Godavari, and Krishna rivers, was observed in the western part of the BOB (Colin et al., 1999). Naidu et al. (1985) reported that smectite (29 % to 44 %) and illite (30 % to 38 %) are dominant of the Mahanadi river, while smectite is dominant (71 % to 91 %) off the Godavari and Krishna rivers (Raman et al., 1995; Vuba et al., 2015). Clay minerals in northeastern BOB and the Andaman Sea are characterized by high smectite content (45 % to 86 %), which may be from the IBA Ranges and the Irrawaddy river (Joussain et al., 2016).

3. Material and methods

3.1. IODP Site U1445

IODP Site U1445 (17°44.72′N, 84°47.25′E; 2513 m water depth), consisting of three drilled holes (Holes U1445A, U1445B, and U1445C), was located in the Mahanadi Basin of the northwestern BOB (Fig. 1b). Visual core descriptions, smear slide examinations, physical properties, and X-ray diffraction data were compiled to describe the lithostratigraphic unit (~672 m long) at Site U1445 (Clemens et al., 2016). Overall, the sediments were homogenous and mainly consisted of hemipelagic clays, including biogenic components intercalated occasionally with thin turbidites. In this study, samples were collected at the uppermost part (from ~ 0.04 to ~ 35 m CCSF-A) of two holes (Holes U1445A and U1445C), generally avoiding the turbidite sediment layers to obtain a complete composite core. All analytical data are summarized in Supplement Data.

3.2. Radiocarbon age dating

The mixed planktonic foraminifera (*Globigerina sacculifer, Globigerinoides ruber*, and *Globorotalia menardii*, sized range: >350 μm) from the three horizons at the uppermost part were picked for Accelerated Mass Spectrometer (AMS) ^{14}C dating at Beta Analytic (USA) (Table 1). All the conventional radiocarbon dates were converted to the calendar ages using the BetaCal3.21 software and the MARINE13 dataset (Reimer et al., 2013), following the global ocean reservoir effect of 400 years (Stuiver and Reimer, 1993) and a local reservoir correction (ΔR) of −60 years (Dutta et al., 2001).

3.3. Oxygen and carbon isotopes

In this study, 109 samples were selected to measure the δ^{18}O and δ^{13}C values of planktonic foraminifera (*G. ruber*). Large test-sized (250–355 μm) foraminifera was collected from the > 150 μm size fraction to minimize the effect of ontogenetic and growth rate on isotopic values (Spero et al., 2003). Before the measurement, cleaning of shell tests was conducted following the method described in Barker et al. (2003). The oxygen and carbon isotope compositions of weighed foraminifera samples (approximately 70–100 μg) were measured using IsoPrime isotope ratio mass spectrometry at the Center for Advanced Marine Core Research of Kochi University (Japan). The isotope ratios were calibrated to the Vienna Pee Dee belemnite (V-PDB) standard using the international standard IAEA-603. The analytical precision of the δ^{18}O and δ^{13}C values was ± 0.05 ‰ and ± 0.02 ‰, respectively.

The carbon isotope composition ($\delta^{13}C_{SOM}$) of the sediment organic matter was measured for the selected 150 sediment samples using elemental analysis-isotope ratio mass spectrometry (EA-IRMS: Europa Scientific 20–20 isotope ratio mass spectrometer) at IsoAnalytical ltd. (UK). Before $\delta^{13}C_{SOM}$ analysis, sediment samples were acidified with 1 M HCl to remove carbonate components. Subsequently, the samples were ground after being neutralized with distilled water and oven-dried at 60℃. In the final step, tin capsules containing the residual sediment powder or reference material were loaded into an auto-sampler of the EA-IRMS. The resultant CO_2 chromatographic peaks were measured using the ion source of EA-IRMS. IA-R001, IA-R005, and IA-R006 as reference materials were used during the $\delta^{13}C_{SOM}$ analysis. The $\delta^{13}C_{SOM}$ values were expressed in conventional delta notation, which is the per mil deviation from the V-PDB standard. The analytical precision for $\delta^{13}C_{SOM}$ was approximately ± 0.08 ‰.

3.4. Detrital Nd and Sr isotopes

Nd and Sr isotopes of the detrital silicate fraction were measured for the selected 38 bulk sediments using a Thermal Ionization Mass Spectrometers (TIMS) of GVI IsoProbe-T and VG Sector 54–30, respectively, at Nagoya University (Japan). First, the carbonate, Fe-Mn oxide, and biogenic silica components within the sediments were removed using 1.5 M acetic acid, 0.05 M hydroxylamine hydrochloride in 25 % acetic acid, and 1 M sodium hydroxide, respectively. Subsequently, ~50 mg of each dried residue was dissolved using a mixture of concentrated HF, HNO_3, and $HClO_4$ (TAMAPURE-AA-100 from Tama Chemicals, ltd., Tokyo), and the chemical separation of Nd and Sr was achieved with conventional column chemistry. The Nd isotope standard JNdi-1 and Sr isotope standard NIST-SRM 987 were $^{143}Nd/^{144}Nd = 0.512115 \pm 0.000011$ (2σ, n = 12) and $^{87}Sr/^{86}Sr = 0.710261 \pm 0.000009$ (2σ, n = 14), respectively. All reported Nd ($^{143}Nd/^{144}Nd$) and Sr ($^{87}Sr/^{86}Sr$) isotope ratios were normalized to $^{146}Nd/^{144}Nd = 0.7219$ and $^{86}Sr/^{88}Sr = 0.1194$, respectively. The Nd isotope ratios are expressed as ε_{Nd}, calculated using a $^{143}Nd/^{144}Nd$ value of 0.512638 for the CHUR (Chondritic Uniform Reservoir: Hamilton et al. (1983)), as follows.

$$\varepsilon_{Nd} = \left[\left({}^{143}Nd/{}^{144}Nd \right)_{sample} / 0.512638 - 1 \right] \times 10000$$

3.5. Clay mineral compositions

Seventy-six sediments were selected to measure the clay minerals of the fine-grained particles (less than2 μm) using X-ray diffraction (XRD: Siemens/Bruker D5005) with Cukα Ni-filtered radiations at Gyeongsang National University (Korea). Before scanning, the 10 % H_2O_2 was used to remove organic matters from the bulk sediments. Then, the clay particles (less than2 μm) were separated by the sedimentation based on Stokes' Law. The air-dried and ethylene-glycolated oriented mounts were prepared using the "smear-on glass slide" method (Stokke and Carson, 1973). Identifying clay minerals was based on the basal reflections recorded in the XRD traces and the guidelines in Brown and

Table 1
AMS ^{14}C dating results of the mixed planktonic foraminifera at Site U1445.

Sample information	Depth (CCSF-A m)	^{14}C age (year BP)	Calibrated age (cal. year BP)	species	Lab ID
U1445C 1H2W 44–46 cm	0.02–0.04	10,920 ± 30	12,293	*G. sacculifer, G. ruber*	Beta-556830
U1445A 1H3W 126–128 cm	2.18–2.20	13,710 ± 50	15,788	*G. sacculifer, G. ruber*	Beta-556831
U1445C 2H1W 140–142 cm	3.97–3.99	26,440 ± 80	29,876	*G. sacculifer, G. ruber, G. menardii*	Beta-556832

Brindley (1980) and Moore and Reynolds (1989). The XRD peak areas of the four main clay minerals (smectite, illite, kaolinite, and chlorite) were estimated by a semi-quantitative calculation (weighted peak area %) in the glycolated state using Eva 3.0 software with the empirical factors of the Biscaye (1965). The overall analytical precision for the clay mineral estimation was approximately ± 5 %.

3.6. Geochemical properties and their mass accumulation rate

To measure the geochemical properties of the sediments, 300 samples were collected. The total carbon (TC) and total nitrogen (TN) contents were measured using a Flash 2000 Series Elemental Analyzer at Pusan National University (Korea) with an analytical precision of less than ± 0.1 % and ± 0.01 %, respectively. The total inorganic carbon (TIC) content was measured using a UIC CO_2 Coulometer (Model CM5240) at Korea Polar Research Institute (Korea). The TIC content was used to calculate the $CaCO_3$ content as a percentage by weight with a multiplication factor of 8.333 (the molecular weight ratio between $CaCO_3$ and C), assuming that all carbonate had been generated from $CaCO_3$. The total organic carbon (TOC) content was calculated as the difference between TC and TIC content.

Analysis of the biogenic silica (Si_{Bio}) content followed a wet alkaline extraction method modified from DeMaster (1981). In principle, the wet alkaline extraction method is based on the idea that biogenic silica and terrestrial aluminosilicates have different dissolution rates in a weakly alkaline solution. The weighed samples (~12–15 mg) were transferred to 50 ml centrifuge tubes with 30 ml of 1 M NaOH and placed in an 85℃ hot water bath. At every hour from 2 h to 5 h, the time-course supernatant sample (i.e., dissolved silica) was pipetted from the hot solution. The dissolved silica concentration that was finally extracted by the wet alkaline extraction method was measured using the molybdenum-blue spectrophotometric method on a Continuous Flow Analyzer (SKALAR SANplus Analyzer) at KOPRI (Korea). The relative error of the biogenic silica concentration was less than 1 %. The biogenic opal content was calculated by multiplying the Si_{Bio} content by 2.4 (Mortlock and Froelich, 1989).

The mass accumulation rate (MAR) of TOC, $CaCO_3$, and biogenic opal was calculated as follows: Biogenic component MAR ($g/cm^2/kyr$) = biogenic component content × dry bulk density (DBD; g/cm^3) × linear sedimentation rate (LSR; cm/kyr). The DBD was measured onboard from discrete samples at approximately 3 m intervals (Clemens et al., 2016). The LSR was calculated based on the slope of the age-depth plot at each interval.

4. Results

4.1. Age model

The chronology at Site U1445 was established with the 3 AMS ^{14}C dates, $\delta^{18}O_{G.\ ruber}$ stratigraphy, and Toba ash layer (Fig. 2). The sediments with ages younger than the oldest AMS ^{14}C date (26,440 year B.P.) were determined by extrapolating the linear sedimentation rates between the dated depths. The core chronology older than 26.4 kyr B.P. was constructed with reference to the correlation between the $\delta^{18}O_{G.\ ruber}$ stratigraphy and SPECMAP (Martinson et al., 1987). In addition, the volcanic ash layer at 14.9 m CCSF-A, identified as the Youngest Toba Tuff (YTT; ~75 ka), was used (Storey et al., 2012). As a result, the study interval (~35 m CCSF-A) of the composite core covered the last two complete glacial-interglacial cycles (~200 kyrs) spanning Marine Isotope Stage (MIS) 1 to 6 and a part of MIS 7 (Fig. 2).

4.2. Nd and Sr isotopes of detrital particles and clay minerals of fine-grained sediments

The ε_{Nd} values and $^{87}Sr/^{86}Sr$ ratios of the detrital fraction of bulk sediments at Site U1445 ranged from −18.6 to −14.1 and from 0.731 to 0.753, respectively (Fig. 3a and b). Both isotope data were within the ranges of the detrital particles derived from the GBM rivers (ε_{Nd} values: −21.3 to −12.5 and $^{87}Sr/^{86}Sr$ ratios: 0.720 to 0.802) (Singh and France-Lanord, 2002; Lupker et al., 2013; Awasthi et al., 2018), and were comparable to the previous reported data in western BOB, where the terrigenous sediments were mainly supplied through the river systems of the Himalaya and Peninsular India (Colin et al., 1999; Ahmad et al., 2009). Downcore fluctuations in the ε_{Nd} values were not synchronous with the interglacial and glacial cycles. In contrast, the slightly higher $^{87}Sr/^{86}Sr$ ratios were discernible during the interglacial periods (MIS 1, 3, and 5) than during the glacial periods (MIS 2, 4, and 6).

Illite content was highest (46 %–73 %), followed by smectite (3 %–34 %), kaolinite (10 %–20 %), and chlorite (7 %–16 %) at Site U1445. These results are similar to the previous results in the BOB (Li et al., 2018). In general, the levels of illite and chlorite were opposite to those of smectite (Fig. 3c and d). The illite and chlorite content was relatively higher during the glacial periods, whereas the smectite content was higher during the interglacial periods. The smectite/(illite + chlorite) [S/(I + C)] ratios varied between 0.04 and 0.62, showing the contrasting change between the interglacial higher ratios (MIS 1, 5, and 7, except for MIS 3) and the glacial lower ratios (MIS 2, 4, and 6) (Fig. 3g).

4.3. Geochemical properties and $\delta^{13}C_{G.ruber}$ and $\delta^{13}C_{SOM}$ values

During the last 200 kyrs, the TOC content at Site U1445 fluctuated from 0.6 % to 2.3 %; the higher values (0.7 %–2.3 %, av. 1.5 %) were observed during the interglacial periods and the lower values (0.6 %–1.9 %, av. 1.2 %) during the glacial periods (Fig. 4a). Variation in the biogenic opal content followed the same pattern as the TOC content, with a higher content (0.8 %–13.1 %, av. 5.6 %) during the interglacial periods and lower content (0.1 %–6.3 %, av. 2.4 %) during the glacial periods (Fig. 4b). In contrast, variations in $CaCO_3$ content were opposite to those of TOC and biogenic opal contents; high contents (2.5 %–64.8 %, av. 26.2 %) were observed during the glacial periods (Fig. 4c). The MARs of TOC, biogenic opal, and $CaCO_3$ varied in parallel each other (Fig. 4a–c: red line). The C/N ratios (9–20, av. 11) were not noticeably different between the interglacial and glacial periods, despite being relatively higher during the glacial periods (Fig. 4d). Similar to the C/N ratios, the variation patterns of $\delta^{13}C_{SOM}$ (-21.1 ‰ to −17.2 ‰) and $\delta^{13}C_{G.ruber}$ (0.3 ‰ to 1.3 ‰) values indicated higher values during the glacial periods (Fig. 4e and f).

5. Discussion

5.1. Land-sea interaction induced by the Indian monsoon variability in the Mahanadi Basin during the last 200 kyrs: Detrital sediment provenance and weathering activity

The ε_{Nd} values and $^{87}Sr/^{86}Sr$ ratios of detrital particles have been used widely as a potential tracer for sediment sources owing to the different lithologies in the drainage basins of rivers around the BOB (Colin et al., 1999; Kessarkar et al., 2005; Tripathi et al., 2011; Joussain et al., 2016; Bretschneider et al., 2020). The downcore ε_{Nd} values at Site U1445 were not visibly different between the interglacial (MIS 1, 3, and 5; −18.6 to −14.2) and glacial (MIS 2, 4, and 6; −17.5 to −14.1) periods (Fig. 3a). However, the $^{87}Sr/^{86}Sr$ ratios were slightly higher during the interglacial periods

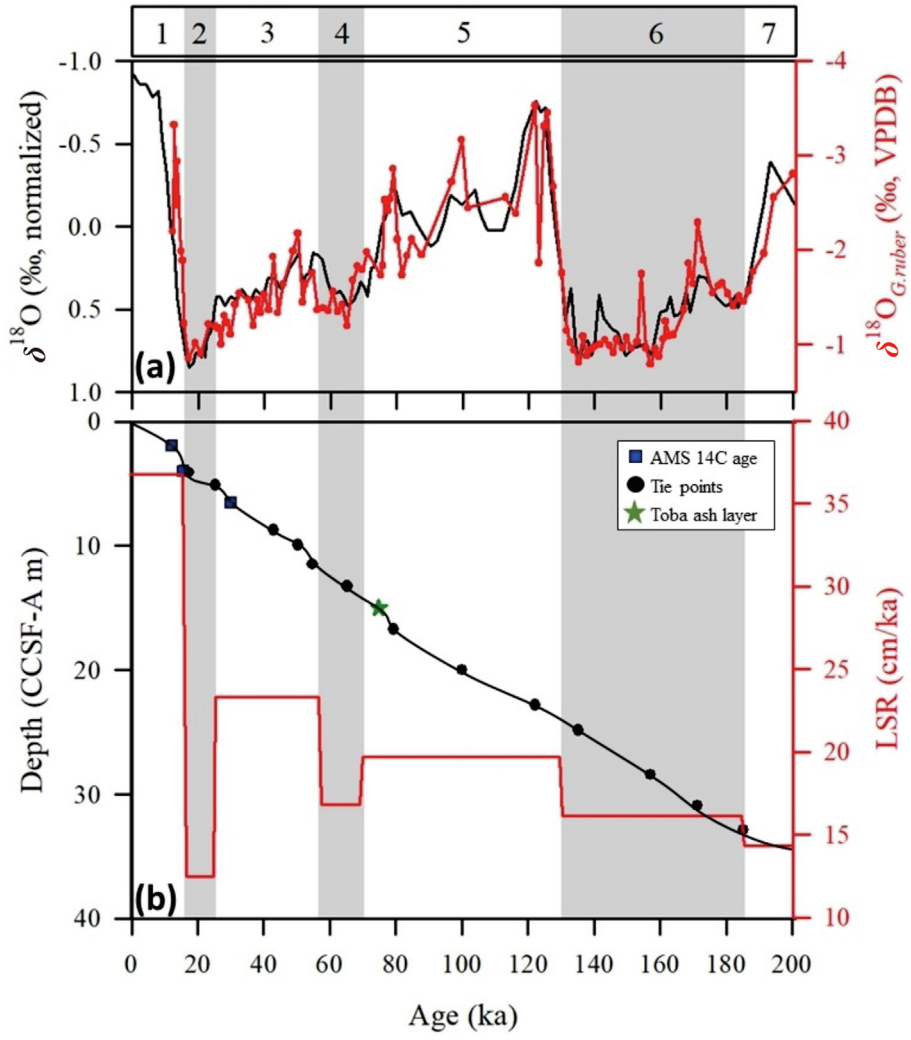

Fig. 2. (a) Age determination by correlation of the $\delta^{18}O_{G.ruber}$ between Site U1445 records (red line) and the SPECMAP records (black line; Martinson et al., 1987). (b) Age-depth diagram of Site U1445 based on the 3 AMS ^{14}C dates (blue squares), tie points from the correlation between $\delta^{18}O_{G.ruber}$ of Site U1445 and SPECMAP (black circles), and Toba ash layer (green star; Storey et al., 2012) with the sedimentation rate (red line) (For interpretation of the references to color in this figure legend, the reader is referred to the web version of this article).

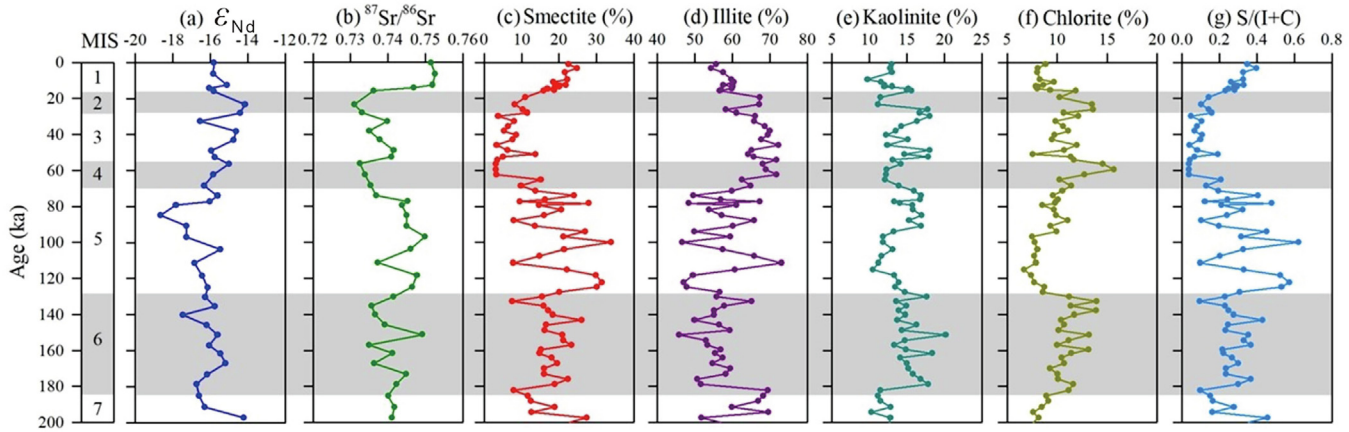

Fig. 3. Downcore variations in (a) ε_{Nd} values, (b) $^{87}Sr/^{86}Sr$ ratios, (c) smectite content, (d) illite content, (e) kaolinite content, (f) chlorite content, and (g) S/(I + C) ratios at Site U1445 over the last 200 kyrs. MIS: marine isotope stage.

(*ca.* 0.744) than during the glacial periods (*ca.* 0.738). Aside from the sediment provenance, the $^{87}Sr/^{86}Sr$ ratios of detrital particles are affected by grain size fraction which is characterized by less radiogenic values in the coarser-grained particles (Meyer et al., 2011), as reported in the BOB and Andaman Sea (Joussain et al., 2016; Lee et al., 2020a). In contrast, Nd isotopic composition is

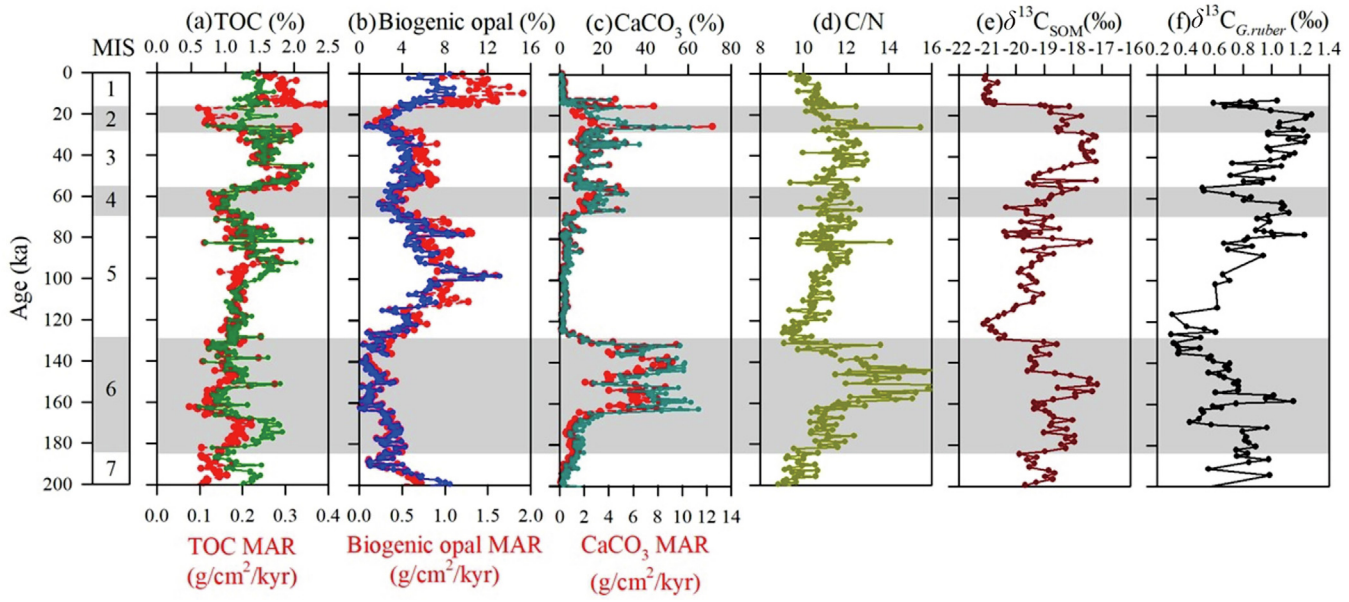

Fig. 4. Downcore variations in (a) TOC content (color) and MAR (color), (b) biogenic opal content (color) and MAR (color), (c) $CaCO_3$ content (color) and MAR (color), (d) C/N ratio, (e) $\delta^{13}C_{SOM}$ values, and (f) $\delta^{13}C_{G.ruber}$ values at Site U1445 over the last 200 kyrs. MIS: marine isotope stage.

mainly unaffected by grain size variations (Meyer et al., 2011). Joussain et al. (2016) reported that the mean grain size was larger in the glacial sediments than the interglacial sediments in the BOB. Under the low sea level conditions during the glacial periods, the transport of coarser particles to the deep basins of the BOB increased due to the reduced distance from the river mouth and the frequent occurrence of turbidity current (Li et al., 2019). Thus, the lower $^{87}Sr/^{86}Sr$ ratios at Site U1445 during the glacial periods are likely attributed to the increased influx of coarser detrital particles into the Mahanadi Basin, although the careful sampling avoids the turbidite layers (Fig. 3b).

Fig. 5 compares the Nd-Sr isotopic data of Site U1445 with those of potential source areas such as the GBM, Mahanadi, Krishna, Godavari, Irrawaddy rivers, and IBA Ranges (described in section 2.2). According to the previous Nd-Sr isotope studies, sediments in the eastern BOB are mainly supplied from the GBM rivers (ε_{Nd} values, −21.3 to −12.5 and $^{87}Sr/^{86}Sr$ ratios, 0.720 to 0.802) and IBA Ranges/Irrawaddy river (ε_{Nd} values, −8.9 to −2.0 and $^{87}Sr/^{86}Sr$ ratios, 0.702 to 0.712) (Joussain et al., 2016). In contrast, those in the western BOB are mainly supplied by the Mahanadi, Krishna, and Godavari rivers (ε_{Nd} values, −18.2 to −12.0 and $^{87}Sr/^{86}Sr$ ratios, 0.719 to 0.730), including the GBM rivers (Colin et al., 1999; Li et al., 2017, 2018). The isotope data at Site U1445 were plotted closer to those for the sediments of the western BOB (Fig. 5). However, it should be noted that all Nd-Sr isotope data at Site U1445 were plotted as a cluster within the range of GBM rivers, falling far from the Mahanadi, Krishna, and Godavari rivers. In addition, our average Nd-Sr isotopes data are similar to those of the BOB shelf and the middle Bengal Fan sediments that originated from the GBM river system (Lupker et al., 2013). The sediment contribution from the Krishna and Godavari rivers in the study area through the longshore sediment transport may be insignificant because the annual net direction of sediment transport is southward (Chandramohan and Nayak, 1991). In addition, scatter diagram of our Nd-Sr isotopes does not show any noticeable contribution of the Mahanadi river sediments, although Site U1445 was located in the Mahanadi Basin. These results indicate that the GMB river system is the dominant factor supplying sediments to the study area. In summary, Nd-Sr isotopic systematics at Site U1445 show that sediment provenance in the Mahanadi Basin has not changed significantly

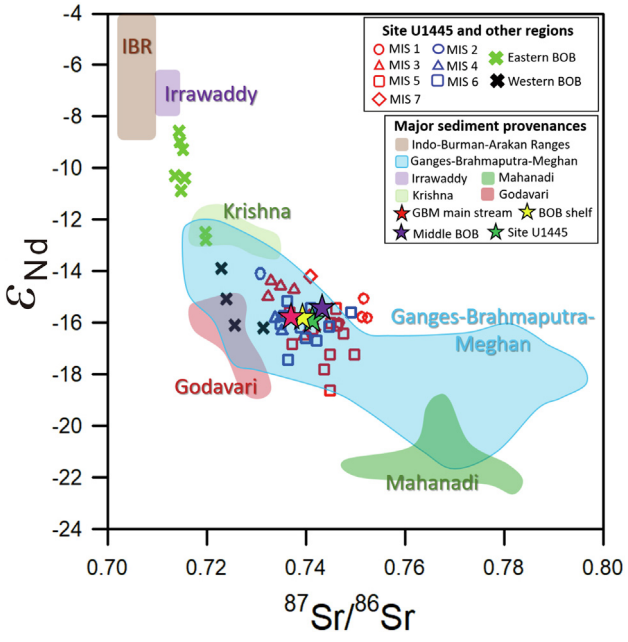

Fig. 5. Biplot of ε_{Nd} values and $^{87}Sr/^{86}Sr$ ratios at Site U1445 with potential major source regions adjacent to the BOB, including IBA Ranges (Awasthi et al., 2014), Irrawaddy (Giosan et al., 2018), Ganges-Brahmaputra-Meghan (Singh and France-Lanord, 2002; Lupker et al., 2013; Awasthi et al., 2018), Mahanadi (Peketi et al., 2021), Krishna (Ahmad et al., 2009), Godavari (Ahmad et al., 2009) rivers and other sediment core data recorded in the eastern BOB (bright green cross; Joussain et al., 2016) and the western BOB (black cross; Colin et al., 1999). Average Nd-Sr isotopic values at Site U1445 (this study: green star), GBM main stream (red stars), BOB shelf (yellow stars), and middle BOB (purple star) (Lupker et al., 2013) (For interpretation of the references to color in this figure legend, the reader is referred to the web version of this article).

between the interglacial and glacial periods during the past 200 kyrs, although the Sr isotopic compositions were slightly affected by the grain size.

The clay mineral assemblages in the BOB were influenced by sediment sources and/or the degree of chemical weathering in

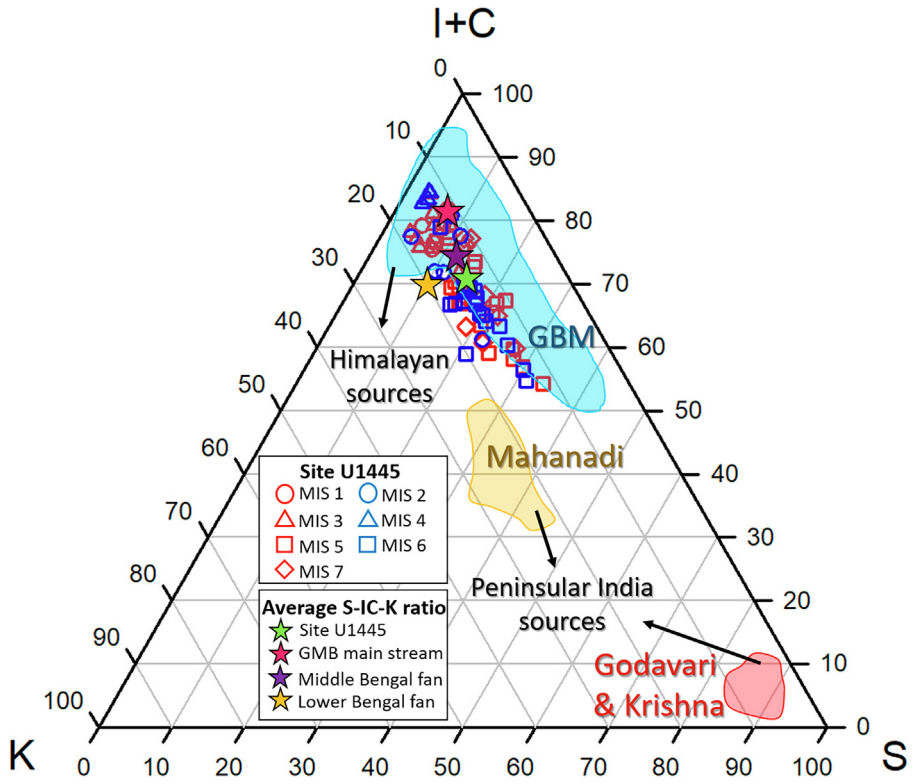

Fig. 6. Ternary diagram of S-IC-K at Site U1445 with major sources of fine-grained sediments, including GBM river systems (Khan et al., 2019), Mahanadi (Naidu et al., 1985), Krishna/Godavari (Raman et al., 1995; Vuba et al., 2015) rivers. Average of S-IC-K ratio at Site U1445 (this study: green star), GBM main stream (red star; Khan et al., 2019), middle Bengal Fan (purple star; Li et al., 2017), and lower Bengal Fan (orange star; Sun et al., 2020) (For interpretation of the references to color in this figure legend, the reader is referred to the web version of this article).

the source regions caused by climatic change (Joussain et al., 2016; Li et al., 2017, 2018; Sun et al., 2020). Based on the Nd/Sr isotope systematics, we confirmed that sediment provenances at Site U1445 have not changed dramatically in the past 200 kyrs (Fig. 5). Thus, a ternary diagram of smectite-(illite + chlorite)-kaolinite [S-IC-K] can also be used to reliably identify the source of sediments in the BOB (Phillips et al., 2014; Joussain et al., 2016; Li et al., 2017, 2018; Sun et al., 2020). Fig. 6 compiles the clay mineral assemblages at Site U1445 with potential source areas; the GBM, Mahanadi, Godavari, and Krishna rivers were found to be the major sources of fine-grained particles in the northern and western BOB regions (described in section 2.2). A ternary diagram of S-IC-K illustrates that the clay minerals at Site U1445 contain the different contributions between the Himalayan rivers (i.e., GBM rivers) and the Peninsular India rivers (i.e., Mahanadi, Godavari, and Krishna rivers) (Fig. 6). All the samples at Site U1445 were clustered in a group of the GBM rivers representative of the Himalayan source without a large discrepancy between the glacial and interglacial periods (Fig. 6). However, these data at Site U1445 was plotted far from the Mahanadi, Godavari, and Krishna rivers (i.e., Peninsular India source). In addition, the average clay mineral contents at Site U1445, illite (61 %), smectite (15 %), kaolinite (14 %), and chlorite (10 %), are similar to those of the middle and lower Bengal Fan sediments, which has a dominant contribution to sediments from the GBM rivers (Fig. 6: Li, et al., 2017; Sun et al., 2020). Thus, the result of the ternary diagram of S-IC-K supports a strong contribution of fine-grained sediments to Site U1445 from the GBM river systems during the past 200 kyrs.

Based on the Nd-Sr isotopic systematics and the ternary diagram of S-IC-K ratios at Site U1445, sediments in the Mahanadi Basin have mainly originated from the Himalayas (GBM rivers) during the past 200 kyrs, although the core site seems influenced by the Mahanadi river. Milliman and Farnsworth (2001) reported that the sediment contribution by the Peninsular India rivers (~60 Mt/yr) is extremely minor, compared with the GBM rivers (>1000 Mt/yr). In addition, a large amount of sediments from the Mahanadi river may be captured within the subaqueous delta and inner continental shelf during the high sea-level interglacial periods, resulting in a little sediment supply directly transported to the offshore in the Mahanadi Basin. Li et al. (2019) suggested that the depositional center in the central BOB varied between the Holocene and the last glacial period, resulting in more sediment deposition in the Bengal Fan during low sea level conditions. Consequently, the principal sediment source at Site U1445 may be the GBM rivers without dramatic change during the last 200 kyrs.

Because detrital sediment provenance in the Mahanadi Basin has not changed significantly since 200 ka (Figs. 5 and 6), the variation of clay mineral compositions at Site U1445 should be related to the weathering activity in the source regions (i.e., drainage regions of GBM rivers) in response to climatic conditions. Climate factors such as temperature and precipitation have played an essential role in controlling weathering patterns through physical erosion and chemical weathering (Meyer et al., 2011), which strongly affects clay mineral assemblages of siliciclastic sediments (e.g., Colin et al., 1999). Illite and chlorite are mainly produced by the physical erosion of igneous and metamorphic rocks under cold and dry climatic conditions. In contrast, smectite and kaolinite are created by enhanced chemical weathering under warm and humid climatic conditions (Chamley, 1989). Consequently, smectite/(illite + chlorite) [S/(I + C)] ratios at Site U1445 can be used as a proxy to trace the degree of weathering activity in the drainage basins of the GBM river systems in response to climatic changes; high ratios due to the intense chemical weathering caused by warm and humid conditions and *vice versa* by cold and dry conditions.

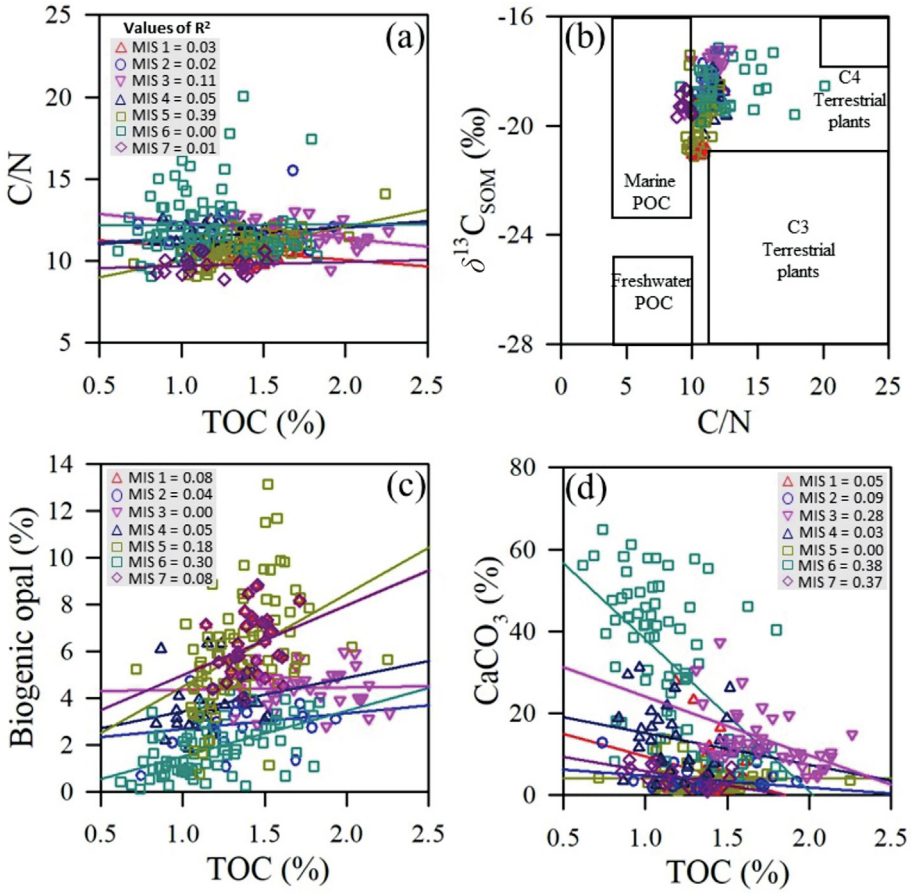

Fig. 7. Correlation between (a) TOC content and C/N ratios, (b) C/N ratios and $\delta^{13}C_{SOM}$ values, (c) TOC content and biogenic opal content, and (d) TOC content and $CaCO_3$ content at Site U1445.

To further confirm the potential association between weathering patterns and paleoclimatic changes between the interglacial-glacial cycles, we compared the variability of S/(I + C) ratios at Site U1445 between MIS 1 (interglacial period) and MIS 2 (glacial period) with the speleothem $\delta^{18}O$ data from northern India (Bittoo Cave; Kathayat et al., 2016) and salinity records from the northern BOB (SO93-126KL; Kundrass et al., 2001), representing the variation of ISM intensity (Fig. 8a–c). It was reported that the decreasing $\delta^{18}O$ values of Bittoo Cave speleothem in northern India and the lower salinity in the surface waters of the northern BOB resulted from the increase in ISM precipitation from MIS 2 to MIS 1 (Kathayat et al., 2016; Kundrass et al., 2001). Although our results do not coincide precisely with speleothem and salinity records, presumably due to the different sampling resolution, S/(I + C) ratios at Site U1445 are different between MIS 1 and MIS 2. Therefore, the enhanced chemical weathering during MIS 1 relative to MIS 2 in the drainage basins of the GBM river systems was closely related to the heavier precipitation induced by the strong ISM (SW monsoon) and/or weak Indian winter monsoon (IWM; NE monsoon) during MIS 1 as compared with MIS 2 (Fig. 8a–c). Our results are in good agreement with the previous findings on the increase of chemical weathering after MIS 2 in the BOB (Colin et al., 1999; Phillips et al., 2014).

5.2. Land-sea interaction induced by Indian monsoon variability in the Mahanadi Basin during the last 200 kyrs: Paleoproductivity variations

Measuring the C/N ratios of sediments allows distinguishing the origin of organic matter within sediments (Meyers, 1994), which are characterized by different ratios between marine organic matter (phytoplankton; 5–10) and terrestrial vascular plants (>12). The range (9–20, av. 11) of C/N ratios at Site U1445 implies a mixture of marine and terrestrial organic matter within the sediments, although it was difficult to estimate the contribution of terrestrial organic matter in the study area because of the statistically poor correlation coefficients (Fig. 7a). Similarly, $\delta^{13}C_{SOM}$ values also confirmed a mixture of those organic materials at Site U1445 (Fig. 7b). However, we demonstrated that the variation patterns of C/N ratios and $\delta^{13}C_{SOM}$ values showed a relatively increasing trend during the glacial periods (Fig. 4, e). Considering that the global sea level was lower during the glacial periods (Grant et al., 2014), the higher C/N ratios may be attributed to the increased contribution of terrigenous organic matters, suggesting that the variation of C/N ratios was not driven by the change of ISM strength. On the other hand, variation of $\delta^{13}C_{SOM}$ values during the glacial-interglacial cycles was affected by atmospheric CO_2 concentration, air temperature, and the relative abundance of C3 and C4 vegetation (references in Yamamoto et al., 2022). Yamamoto et al. (2022) reported that photosynthesis of C3 plants was suppressed relative to photorespiration in low CO_2 conditions (i.e., glacial periods), indicating that C4 plants take an advantage over C3 plants during the glacial periods. For example, Phillips et al. (2014) suggested that the higher $\delta^{13}C_{SOM}$ values during the glacial periods resulted from the C4 plant dominance under the drier conditions by weakened ISM (SW monsoon) precipitation in the northwestern BOB. In addition, potential variation in marine productivity can also affect the changes of $\delta^{13}C_{SOM}$ value in marine sediment (Lamb et al., 2006). In the lower Bengal Fan, it was observed that the $\delta^{13}C_{SOM}$ value of sediments was high when the marine production increased during the glacial

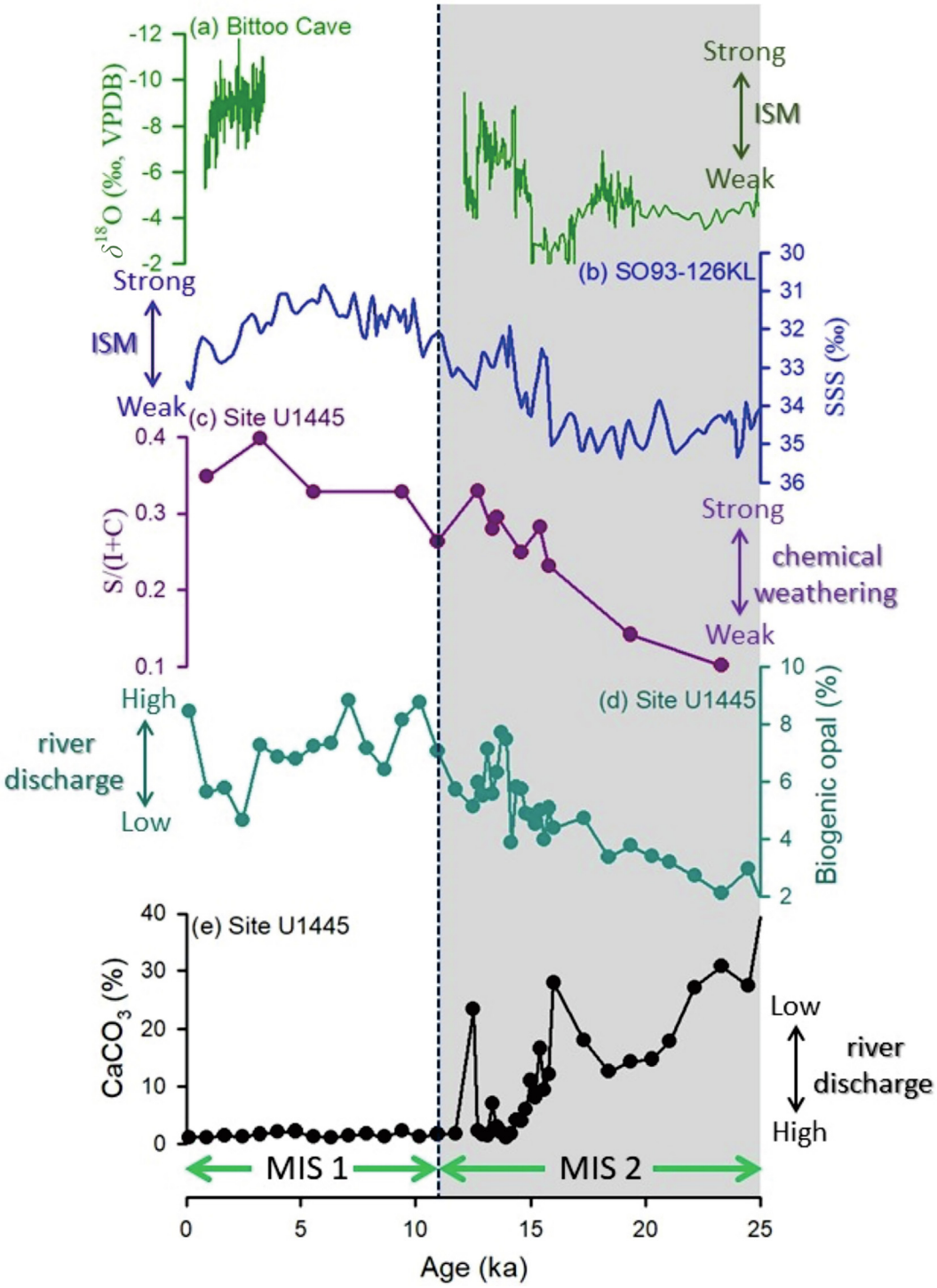

Fig. 8. Comparison of proxy records of paleoclimatic changes such as ISM intensity and paleoceanographic records at Site U1445 from the glacial (MIS 2) to interglacial (MIS 1) periods. (a) Speleothem $\delta^{18}O$ record from Bittoo Cave in northern India (Kathayat et al., 2016), (b) sea surface salinity (SSS) record from SO93-126KL core in the northern BOB (Kundrass et al., 2001), (c) weathering intensity based on S/(I + C) ratios at Site U1445 (this study) and (d) river discharge record based on biogenic opal at Site U1445 (this study), (e) river discharge record based on $CaCO_3$ content at Site U1445 (this study).

periods, which was associated with weak stratification of surface waters (Weber et al., 2018). Consequently, the higher $\delta^{13}C_{SOM}$ values during the glacial periods could be the result of either increased marine production or a shift in terrestrial plant biomass to C4 plant dominance under the cold/drier conditions of the weakened ISM (SW monsoon) precipitation and/or strong IWM (NE monsoon). TOC content seemed to be correlated positively with the biogenic opal content and negatively with $CaCO_3$ content (Fig. 7c and d). The higher TOC content and MARs during the interglacial periods may be attributed to the increased biogenic opal productivity (Fig. 4). Ramaswamy and Gaye (2006) reported that diatoms significantly influenced organic carbon fluxes in the BOB. These results suggest that TOC content and MARs at Site U1445 have been mostly related to the biogenic opal production over the last 200 kyrs, despite the contribution of terrestrial organic matters.

The biogenic opal contents and MARs of deep-sea sediments are controlled by the production, dissolution, and preservation. Based on the age model at Site U1445, the sedimentation rate was high (average ~ 21 cm/kyr), which facilitates the preservation of biogenic opal on the deep seafloor (Ragueneau et al., 2000). Moreover, the dissolution of biogenic opal in the Mahanadi Basin was assumed to be relatively constant between 1000 and 3000 m water depth (Nelson et al., 1995), despite difficulty estimating the precise dissolution effect within the water column. Thus, temporal variations in biogenic opal content and MARs at Site U1445 are attributed primarily to changes in biogenic siliceous production in the surface water rather than differential preservation and dissolution. Of the macronutrients, silicate concentration is most important for diatom growth rates (Officer and Ryther, 1980). The BOB received a large amount of dissolved silicate from the GBM rivers and Peninsular India rivers (Prasanna Kumar et al., 2002). Higher silicate concentrations relative to nitrate and phosphate were observed in the low saline waters of the northern BOB, suggesting that riverine freshwater is the primary source of silicate in the BOB (Sarma et al., 2016). Consequently, variations in biogenic opal content and MARs at Site U1445 are closely related to the degree of river discharge, with a positive linkage between diatom production and river runoff.

Similar to biogenic opal, $CaCO_3$ content and MARs in the BOB are also controlled mainly by calcite production and differential preservation (Naidu and Malmgren, 1999). Prasanna Kumar et al. (2007) reported that nitrogen influxes significantly influenced calcareous phytoplankton production in the Indian Ocean. However, nitrate concentration supplied by the rivers is not comparable to silicate concentration, indicating that freshwater runoff is not a major source of nitrate in the BOB (Prasanna Kumar et al., 2002). In contrast, coastal upwelling, especially in the northwestern BOB, is the principal process supplying subsurface nitrate to surface water (Sarma et al., 2016). Significant river runoff intensified the water column stratification, leading to reduced coastal upwelling. In the northwestern BOB, the highest nitrate concentrations were observed during the low riverine discharge season when coastal upwelling increased (Miranda et al., 2020). Thus, we assumed that the $CaCO_3$ content and MARs at Site U1445 were related to the freshwater influx and upwelling activity, verifying that calcareous biogenic production increased under the lower riverine discharge conditions. Moreover, the degree of carbonate preservation (i.e., dissolution) depends on the variations of aragonite compensation depth (ACD). During the Quaternary, the ACD in the northern Indian Ocean was shallower during the interglacial periods (Sijinkumar et al., 2010). Hence, the production and preservation of calcareous marine organisms might be the significant factors contributing to the variation in $CaCO_3$ content and MARs at Site U1445 in the Mahanadi Basin.

Based on the geochemical proxies, the changes in biogenic opal and $CaCO_3$ content changes at Site U1445 were closely related to riverine discharge, with high biogenic opal and low $CaCO_3$ content under high riverine discharge and *vice versa* under low riverine discharge. We confirmed a clear shift from the dominance of $CaCO_3$ deposition during MIS 2 to the dominance of biogenic opal deposition during MIS 1, reflecting an increase in freshwater discharge to the northwestern BOB since MIS 2 (Fig. 8d and e). Our results are also supported by the increase in freshwater discharge to the northern BOB from MIS 2 to MIS 1 (Phillips et al., 2014; Ota et al., 2019), including long-term tectonic timescales (Lee et al., 2020b). For instance, Ota et al. (2019) documented that stratification in the upper water column in the western BOB was stronger during MIS 1 than MIS 2 due to the increased freshwater influx caused by heavy precipitation induced by ISM. The shift in marine plankton community structure-related river discharge was also quite compatible with the strong chemical weathering records at Site U1445, which was caused by stronger ISM (SW monsoon) precipitation during MIS 1 (Fig. 8c). Thus, our results indicate that the variability in marine plankton community structure between MIS 1 and MIS 2 was associated with the change in ISM (SW monsoon) rainfall.

Although all the rhythmic signals do not match identically at the millennial-scale events due to the different sampling resolutions, the hydrological variation patterns have fluctuated similarly throughout the glacial (MIS 2–4 and 6; weak ISM and/or strong IWM)-interglacial (MIS 1, 5, and 7; strong ISM and/or weak IWM) cycles since 200 ka (Fig. 9a and c). The previous studies in the BOB and Andaman Sea also observed a significant decrease in chemical weathering caused by the weakened ISM and/or enhanced IWM intensity during the glacial periods since the penultimate maximum glacial period (i.e., MIS 6) (Colin et al., 1999; Joussain et al., 2016). During the glacial periods, C4 plants and marine production, which lead to high $\delta^{13}C$ values of sediments, increased under prevailing drier conditions and weakened stratification of surface waters due to reduced ISM (SW monsoon) precipitation (Phillips et al., 2014; Weber et al., 2018; Yamamoto et al., 2022). In this regard, the changes of $\delta^{13}C_{SOM}$ values at Site U1445 between the glacial and interglacial periods were also consistent with the hydrological variation patterns derived from the variabilities of weathering and marine plankton community structure over the last 200 kyrs (Fig. 9b).

Because ^{13}C atoms of dissolved inorganic carbon become abundant in the surface seawaters due to the selective use of ^{12}C atoms through photosynthesis, high $\delta^{13}C$ values of planktonic foraminifera reflect the increase in surface water productivity. The $\delta^{13}C_{G.ruber}$ values at Site U1445 can be used as a paleoproductivity proxy in the northwestern BOB. In the BOB, the high productivity during the glacial periods was associated with weak stratification of surface waters due to the reduced freshening by weakened ISM (SW monsoon) precipitation, which supplies nutrients into the euphotic zone (Singh et al., 2011). Weber et al. (2018) also reported that marine primary production in the BOB was elevated during the glacial periods due to the strong upwelling of nutrients since 200 ka. With similar results, the $\delta^{13}C_{G.ruber}$ values at Site U1445 also indicate that surface water productivity increased during the glacial periods (Fig. 9d). In summary, our results demonstrate that the weathering activity and paleoproductivity variations at Site U1445 were closely linked to the intensity of ISM precipitation between the glacial (weak ISM/strong IWM) and interglacial (strong ISM/weak IWM) periods over the last 200 kyrs.

5.3. Effect of the ITF change on the Indian monsoon variability during the last 200 kyrs

Some studies suggested that ISM variability was significantly related to the change of SST in the Indian Ocean over the geological times (Mohtadi et al., 2017; Saraswat et al., 2019; Su et al., 2019), although it has been influenced by multiple factors such as atmospheric CO_2 concentration, global ice volume, Himalayan-Tibetan Plateau uplift, and orbital forcing. The decrease of SST in the Indian Ocean at ~ 3.3 Ma led to environmental changes across Asia, including the phase shift of depositional environment (from lacustrine to fluvial) in the southern Tibetan Plateau and the rapid drying in central Asia (Saylor et al., 2016; Su et al., 2019). In this context, Su et al. (2019) proposed that such a decrease in SST would have reduced heat and moisture levels in the atmosphere, resulting in lower precipitation during both the ISM and East Asian summer monsoon. On orbital timescales, Saraswat et al. (2019) observed that a warmer Indian Ocean during the interglacial periods is synchronous with increased precipitation during the ISM and *vice versa* during the glacial periods. Moreover, several model-

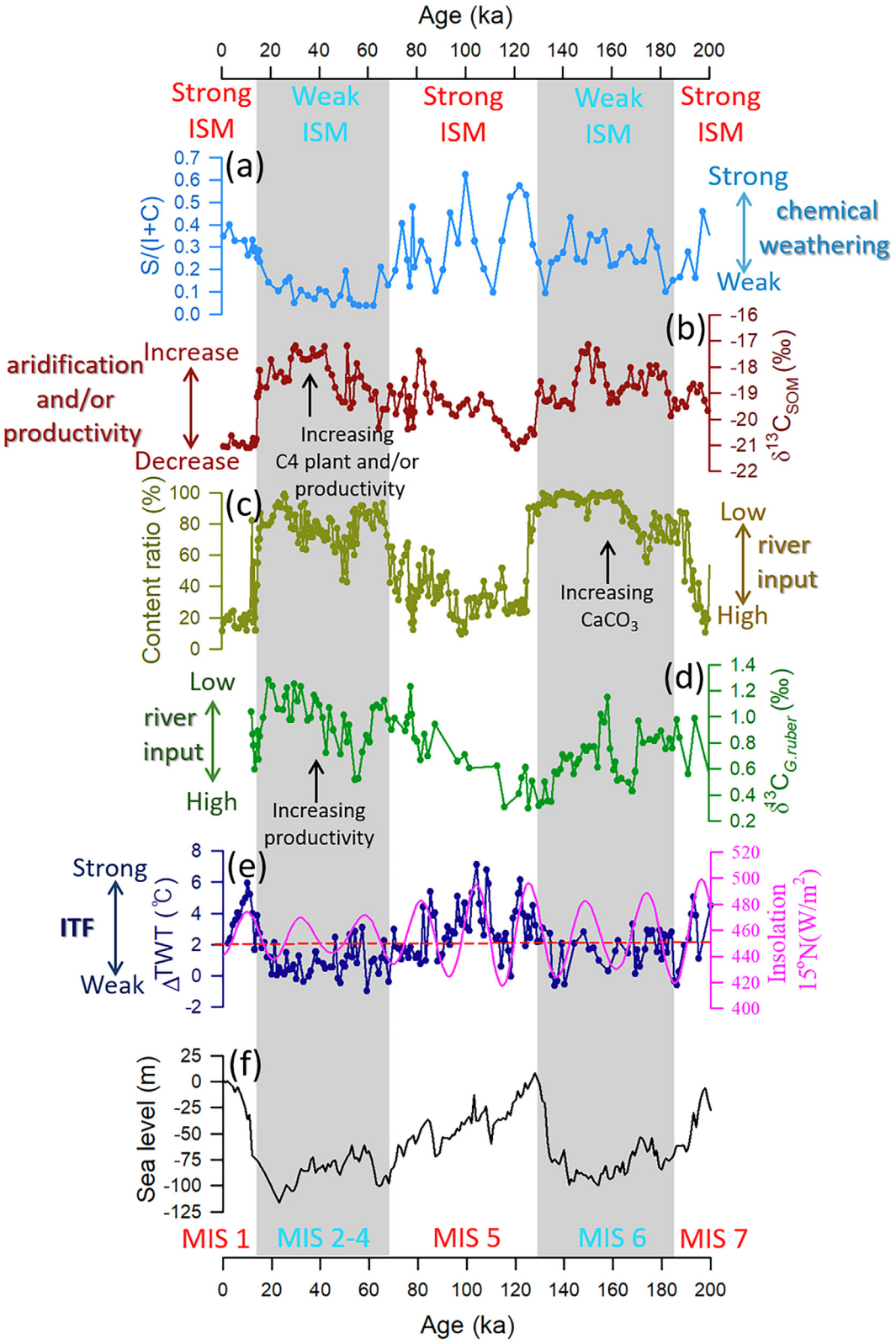

Fig. 9. Evolution of the ISM intensity derived from pale-oceanographic records at Site U1445; (a) S/(I + C) ratios, (b) $\delta^{13}C_{SOM}$ values, (c) $CaCO_3$/biogenic opal content ratio, and (d) $\delta^{13}C_{G.ruber}$ values. The variability of ITF intensity with insolation and global sea-level changes over the last 200 kyrs; (e) Thermocline water temperature (TWT) gradient (dark blue line; Pang et al., 2021) and solar insolation at 15N (pink line; Rachmayani et al., 2016), and (f) global sea-level changes (Grant et al., 2014). (For interpretation of the references to color in this figure legend, the reader is referred to the web version of this article.)

ing studies suggested that the variability of SST anomaly modes in the tropical Indian Ocean, such as the Indian Ocean Basin (IOB) mode and the Indian Ocean Dipole (IOD) mode, is significantly correlated with the ISM intensity at interannual timescales (Yang et al., 2010; Behera and Ratnam, 2018; Chakraborty and Singhai, 2021). Other studies also suggested that positive IOD events

enhanced warming in the western Indian Ocean, which usually occurred under dry conditions over the Indian subcontinent (i.e., weak ISM rainfall) (Meehl and Loschnigg, 2003; Terray et al., 2005), although the linkage between the IOD and ISM intensity remains a controversial issue. Yang et al. (2010) reported that warm IOB (i.e., basin-wide warming of the Indian Ocean) is strongly linked with enhanced ISM rainfall. Thus, such findings imply that change of SST in the Indian Ocean is one of the most important factors regulating ISM variability at orbital and tectonic timescales.

Because the ITF transports substantial heat and moisture from the Pacific to the Indian Ocean, it is considered an important factor affecting SST in the Indian Ocean (Schneider, 1997). According to a modeling study, decreased strength of the ITF increases the reduction of SST in the Indian Ocean (Lee et al., 2002). Jin and Wright (2020) also reported that the ITF, which accounts for about 70%-80% of total ocean advection contribution in the southeastern Indian Ocean, influenced significantly the IOD-IOB transition related to larger SST variance in the eastern Indian Ocean. In particular, a higher SST in the Indian Ocean during the interglacial periods was closely related to the strong westward extension of the Indo-Pacific Warm Pool, leading to warm water transport through the ITF (Saraswat et al., 2019). Thus, based on the observation data and modelling results, SST change in the Indian Ocean is related to changes in the ITF that may shed light on ISM variability. Recently, Pang et al. (2021) reconstructed the strength of ITF over the last 270 kyrs based on the change of TWT gradients (ΔTWT) between core MD98-2165 and SO139-74 KL in the Java upwelling regions (Figs. 1a and 9e). They reported that the ITF was weaker during MIS 2–4 and 6 (i.e., glacial periods) than that during MIS 1, 5, and 7 (i.e., interglacial periods), although the main factors controlling the ITF flux and TWT, such as precession-paced low-latitude insolation and sea level, remain controversial (Fig. 9e, f). Nevertheless, the increase in SST in the Indian Ocean caused by the enhanced ITF intensity is potentially responsible for elevated ISM precipitation during the interglacial periods. In practice, the changing strength of the ITF between the glacial and interglacial periods coincides with our results regarding the hydrological variations over the last 200 kyrs (Fig. 9). Therefore, we contend that our results derived from Site U1445 in the Mahanadi Basin of the northwestern BOB, as weathering activity and paleo-productivity variations, provide robust evidence for the link between ISM precipitation and ITF intensity changes during the glacial-interglacial cycles over the last 200 kyrs.

6. Conclusions

In this study, we reconstructed the weathering activity and paleoproductivity variability recorded at IODP Site U1445 in the Mahanadi Basin of northwestern BOB over 200 kyrs based on multi-proxies including Nd/Sr isotopes, clay mineral compositions, biogenic opal and $CaCO_3$, organic carbon, and carbon isotopes of organic matter. We confirmed that the land–ocean interaction was closely related to the ISM intensity changes over the last 200 kyrs. We revealed that the major sediment sources for study area have not changed significantly during the last 200 kyrs and that the terrigenous particles primarily originated from the GBM rivers system. Thus, the S/(I + C) ratios of clay mineral compositions were used as a proxy to reconstruct the weathering activity during the glacial-interglacial periods. The chemical weathering in the drainage basins of the GBM river systems was enhanced due to the stronger ISM (SW monsoon) precipitation during the interglacial periods (MIS 1, 5, and 6). In addition, we identified a clear shift from the dominance of biogenic opal deposition during the interglacial periods to the dominance of $CaCO_3$ deposition during the glacial periods. During the interglacial periods, diatom production increased as a result of elevated freshwater discharge, supplying high levels of silicates to the BOB. On the other hand, the reduced freshwater discharge during the glacial periods elevated the nitrate supply through increased upwelling, which promoted $CaCO_3$ production. Finally, we suggest that our results regarding the ISM intensity may have been modulated by the variability of ITF strength in terms of low-latitude forcing of climatic changes during the glacial-interglacial cycles over the last 200 kyrs. These results challenge the previous suggestion that the global ice volume as high-latitude forcing of climatic changes plays an important role influencing the ISM variability between the glacial and interglacial periods.

Declaration of Competing Interest

The authors declare that they have no known competing financial interests or personal relationships that could have appeared to influence the work reported in this paper.

Acknowledgments

We thank the crew and shipboard scientists of IODP Expedition 353. We also thank scientists at the sampling party for their assistance in taking core samples which was held during November-December 2009 and March 2010 at Kochi Core Center (Japan). We appreciate KOPRI for allowing the use of analytical machines to measure total inorganic carbon and biogenic opal and Prof. H. G. Cho (Gyeongsang National University) for allowing the use of XRD for the clay mineral analysis. Finally, we appreciate Editorial Advisor (Prof. M. Santosh) and associate editor (Prof. E. Shaji) for their considerable encouragement and three anonymous reviewers for their constructive and thoughtful comments that improved the quality of this manuscript. This research was supported by the National Research Foundation of Korea (2019R1A2C1007701, 2022R1A2B5B01001811) and by the KIOST post-doc fellowship (PEA0023).

References

Ahmad, S.M., Padmakumari, V.M., Babu, G.A., 2009. Strontium and neodymium isotopic compositions in sediments from Godavari, Krishna and Pennar rivers. Curr. Sci. 97, 1766–1769 https://www.jstor.org/stable/24107258.

Awasthi, N., George, B.G., Ray, J.S., 2020. Tracing the sources and depositional pathways for the Oligocene sediments in the Andaman forearc. In: Ray, J., Radhakrishna, M. (Eds.), The Andaman Islands and Adjoining Offshore: Geology, Tectonics and Palaeoclimate. Springer, pp. 93–106. https://doi.org/10.1007/978-3-030-39843-9_5.

Awasthi, N., Ray, J.S., Singh, A.K., Band, S.T., Rai, V.K., 2014. Provenance of the Late Quaternary sediments in the Andaman Sea: Implications for monsoon variability and ocean circulation. Geochem. Geophys. Geosyst. 15, 3890–3906. https://doi.org/10.1002/2014GC005462.

Awasthi, N., Ray, E., Paul, D., 2018. Sr and Nd isotope compositions of alluvial sediments from the Ganga Basin and their use as potential proxies for source identification and apportionment. Chem. Geol. 476, 327–339. https://doi.org/10.1016/j.chemgeo.2017.11.029.

Barker, S., Greaves, M., Elderfield, H., 2003. A study of cleaning procedures used for foraminiferal Mg/Ca paleothermometry. Geochem. Geophys. Geosyst. 4, 8407. https://doi.org/10.1029/2003GC000559.

Behera, S.K., Ratnam, J.V., 2018. Quasi-asymmetric response of the Indian summer monsoon rainfall to opposite phases of the IOD. Sci. Rep. 8, 123. https://doi.org/10.1038/s41598-017-18396-6.

Biscaye, P.E., 1965. Mineralogy and sedimentation of recent deep-sea clay in the Atlantic Ocean and adjacent seas and oceans. Geol. Soc. Am. Bull. 76, 803–832. https://doi.org/10.1130/0016-7606(1965)76[803:MASORD]2.0.CO;2.

Bretschneider, L., Hathorne, E.C., Huang, H., Lübbers, J., Kochhann, K.G.D., Holbourn, A., Kuhnt, W., Thiede, R., Gebregiorgis, D., Giosan, L., Frank, M., 2020. Provenance and weathering of clays delivered to the Bay of Bengal during the Middle Miocene: Linkages to tectonics and monsoonal climate e2020PA003917 Paleoceanogr. Paleoclimatol. 36. https://doi.org/10.1029/2020PA003917.

Brown, G., Brindley, G.W., 1980. X-ray diffraction procedures for clay mineral identification. In: Brindley, G.W., Brown, G. (Eds.), Crystal structures of clay minerals and their x-ray identification. Mineral. Soc. Monogr., London, 5, 305-359. https://doi.org/10.1180/mono-5.5.

Chakraborty, A., Singhai, P., 2021. Asymmetric response of the Indian summer monsoon to positive and negative phases of major tropical climate patterns. Sci. Rep. 11, 22561. https://doi.org/10.1038/s41598-021-01758-6.

Chamley, H., 1989. Clay Sedimentology. Berlin, Germany, Springer-Verlag, 267pp. https://doi. org/10.1007/978-3-642-85916-8_2.

Chandramohan, P., Nayak, B.U., 1991. Longshore sediment transport along the Indian coast. Indian J. Mar. Sci. 20, 110–114.

Chang, C.P., Johnson, R.H., Ha, K.J., Kim, D., Lau, G.N.C., Wang, B., Bell, M.M., Luo, Y., 2018. The Multiscale global monsoon system: research and prediction challenges in weather and climate ES149-ES153 Bull. Am. Meteorol. Soc. 99. https://doi.org/10.1175/BAMS-D-18-0085.1.

Chowdhury, M.R., Ward, N., 2004. Hydro-meteological variability in the greater Ganges-Brahmaputra-Meghna Basins. Int. J. Climatol. 24, 1495–1508. https://doi.org/10.1002/joc.1076.

Clemens, S.C., Kuhnt, W., LeVay, L.J., Anand, P., Ando, T., Bartol, M., Bolton, C.T., Ding, X., Gariboldi, K., Giosan, L., Hathorne, E.C., Huang, Y., Jaiswal, P., Kim, S., Kirkpatrick, J.B., Littler, K., Marino, G., Martinez, P., Naik, D., Peketi, A., Phillips, S. C., Robinson, M.M., Romero, O.E., Sagar, N., Taladay, K.B., Taylor, S.N., Thirumalai, K., Uramoto, G., Usui, Y., Wang, J., Yamamoto, M., and Zhou, L., 2016. Site U1445. In: Clemens, S.C., Kuhnt, W., LeVay, L.J., and the Expedition 353 Scientists, Indian Monsoon Rainfall. Proceedings of the International Ocean Discovery Program, 353: College Station, TX. doi:10.14379/iodp.proc.353.107.2016.

Clift, P.D., Hodges, K.V., Heslop, D., Hannigan, R., Van Long, H., Calves, G., 2008. Correlation of Himalayan exhumation rates and Asian monsoon intensity. Nat. Geosci. 1, 875–880. https://doi.org/10.1038/ngeo351.

Colin, C., Kissel, C., Blamart, D., Turpin, L., 1998. Magentic properties of sediments in the Bay of Bengal and the Andaman Sea: impact of rapid North Atlantic Ocean climatic events on the strength of the Indian monsoon. Earth Planet. Sci. Lett. 160, 623–635. https://doi.org/10.1016/S0012-821X(98)00116-2.

Colin, C., Turpin, L., Bertaux, J., Desprairies, A., Kissel, C., 1999. Erosional history of the Himalayan and Burman ranges during the last two glacial-interglacial cycles. Earth Planet. Sci. Lett. 171, 647–660. https://doi.org/10.1016/S0012-821X(99)00184-3.

Contreras-Rosales, L.A., Jennerjahn, T.C., Tharammal, T., Meyer, V., Lückge, A., Paul, A., Schefuß, E., 2014. Evolution of the Indian Summer Monsoon and terrestrial vegetation in the Bengal region during the past 18 ka. Quat. Sci. Rev. 102, 133–148. https://doi.org/10.1016/j.quascirev.2014.08.010.

DeMaster, D.J., 1981. The supply and accumulation of silica in the marine environment. Geochim. Cosmochim. Acta 45, 1715–1732. https://doi.org/10.1016/0016-7037(81)90006-5.

Devendra, D., Xiang, R., Zhong, F., Yang, Y., Tang, L., 2019. Palaeoproductivity and associated changes in the north-eastern Indian Ocean since the last glacial: Evidence from benthic foraminifera and stable isotopes. J. Asian Earth Sci. 181,. https://doi.org/10.1016/j.jseaes.2019.103913 103913.

Dutta, K., Bhushan, R., Somayajulu, B., 2001. Delta R correction values for the northern Indian Ocean. Radiocarbon 43, 483–488. https://doi.org/10.1017/S0033822200038376.

Giosan, L., Naing, T., Tun, M.M., Clift, P.D., Filip, F., Constantinescu, S., Khonde, N., Blusztajn, J.S., Buylaert, J.-P., Stevens, T., 2018. On the Holocene evolution of the Ayeyawady megadelta. Earth Surf. Dyn. 6, 451–466. https://doi.org/10.5194/esurf-6-451-2018.

Gomes, H.R., Goes, J.I., Saino, T., 2000. Influence of physical processes and freshwater discharge on the seasonality of phytoplankton regime in the Bay of Bengal. Cont. Shelf Res. 20, 313–330. https://doi.org/10.1016/S0278-4343(99)00072-2.

Gordon, A.L., 2005. Oceanography of the Indonesian Seas. Oceanography 18, 14–27. https://doi.org/10.5670/oceanog.2005.01.

Grant, K.M., Rohling, E.J., Bronk Ramsey, C., Cheng, H., Edwards, R.L., Florindo, F., Heslop, D., Marra, F., Roberts, A.P., Tamisiea, M.E., Williams, F., 2014. Sea-level variability over five glacial cycles. Nat. Commun. 5, 5076. https://doi.org/10.1038/ncomms6076.

Hamilton J., P., O'nions K., R., Bridgwater, D., Nutman, A., 1983. Sm-Nd studies of Archaean metasediments and metavolcanics from West Greenland and their implications for the Earth's early history. Earth Planet. Sci. Lett. 62, 263–272. https://doi.org/10.1016/0012-821X(83)90089-4.

Huang, Y., Clemens, S.C., Liu, W., Wang, Y., Prell, W.L., 2007. Large-scale hydrological change drove the late Miocene C4 plant expansion in the Himalayan foreland and Arabian Peninsula. Geology 35, 531–534. https://doi.org/10.1130/G23666A.1.

Jin, X., Wright, J.S., 2020. Contributions of Indonesian Throughflow to eastern Indian Ocean surface variability during ENSO events. Atmos. Sci. Lett. 21, e979 https://doi.org/10.1002/asl.979.

Joussain, R., Colin, C., Liu, Z., Meynadier, L., Fournier, L., Fauquembergue, K., Zaragosi, S., Schmidt, F., Rojas, V., Bassinot, F., 2016. Climatic control of sediment transport from the Himalayas to the proximal NE Bengal Fan during the last glacial-interglacial cycle. Quat. Sci. Rev. 148, 1–16. https://doi.org/10.1016/j.quascirev.2016.06.016.

Kathayat, G., Cheng, H., Sinha, A., Spötl, C., Edwards, R.L., Zhang, H., Li, X., Yi, L., Ning, Y., Cai, Y., Lui, W., Breitenbach, S.F.M., 2016. Indian monsoon variability on millennial-orbital timescales. Sci. Rep. 6, 24374. https://doi.org/10.1038/srep24374.

Kessarkar, P.M., Rao, V.P., Ahmad, S.M., Patil, S.K., Kumar, A.A., Babu, G.A., Chakraborty, S., Rajan, R.S., 2005. Changing sedimentary environment during the Late Quaternary: Sedimentological and isotopic evidence from the distal Bengal Fan. Deep-Sea Res. I 52, 1591–1615. https://doi.org/10.1016/j.dsr.2005.01.009.

Khan, M.H.R., Liu, J., Liu, S., Seddique, A.A., Cao, L., Rahman, A., 2019. Clay mineral compositions in surface sediments of the Ganges-Brahmaputra-Meghna river system of Bengal Basin. Bangladesh. Mar. Geol. 412, 27–36. https://doi.org/10.1016/j.margeo.2019.03.007.

Kida, S., Yamazaki, D., 2020. The mechanism of the freshwater outflow through the Ganges-Brahmaputra-Meghna Delta. Water Resour. Res. 56, e2019WR026412. https://doi.org/10.1029/2019WR026412.

Kundrass, H.R., Hofmann, A., Doose, H., Emeis, K., Erlenkeuser, H., 2001. Modulation and amplification of climatic changes in the Northern Hemisphere by the Indian summer monsoon during the past 80 k.y. Geology 29, 63–66. https://doi.org/10.1130/0091-7613(2001)029<0063:MAAOCC>2.0.CO;2.

Lamb, A.L., Wilson, G.P., Leng, M.J., 2006. A review of coastal palaeoclimate and relative sea-level reconstructions using $\delta^{13}C$ and C/N ratios in orgainc material. Earth Sci. Rev. 75, 29–57. https://doi.org/10.1016/j.earscirev.2005.10.003.

Lee, T., Fukumori, I., Menemenlis, D., Xing, Z.F., Fu, L.L., 2002. Effects of the Indonesian Throughflow on the Pacific and Indian Oceans. J. Phys. Oceanogr. 32, 1404–1429. https://doi.org/10.1175/1520-0485(2002)032<1404:EOTITO>2.0.CO;2.

Lee, J., Kim, S., Lee, J.I., Cho, H.G., Phillips, S.C., Khim, B.-K., 2020a. Monsoon-influenced variation of clay mineral compositions and detrital Nd-Sr istotopes in the western Andaman Sea (IODP Site U1447) since the late Miocene. Palaeogeogr. Palaeoclimatol. Palaeoecol. 538,. https://doi.org/10.1016/j.palaeo.2019.109339 109339.

Lee, J., Kim, S., Khim, B.K., 2020b. A paleoproductivity shift in the northwesten Bay of Bengal (IODP Site U1445) across the Mid-Plestocene transition in response to weakening of the Indian summer monsoon. Palaeogeogr. Palaeoclimatol. Palaeoecol. 560,. https://doi.org/10.1016/j.palaeo.2020.110018 110018.

Li, J., Liu, S., Shi, X., Feng, X., Fang, X., Cao, P., Sun, X., Ye, W., Khokiattiwong, S., Kornkanitnan, N., 2017. Distrubutions of clay minerals in surface sediments of the middle Bay of Bengal: Source and transport pattern. Cont. Shelf Res. 145, 59–67. https://doi.org/10.1016/j.csr.2017.06.017.

Li, J., Liu, S., Liu, X., Zhang, H., Fang, X., Chen, M.T., Cao, P., Sun, X., Ye, W., Wu, K., Khokiattiwong, S., Kornkanitnan, N., 2018. Clay minerals and Sr-Nd isotopic composition of the Bay of Bengal sediments: Implications for sediment provenance and climate control since 40 ka. Quat. Int. 493, 50–58. https://doi.org/10.1016/j.quaint.2018.06.044.

Li, J., Liu, S., Shi, X., Zhang, H., Fang, X., Cao, P., Yang, G., Xue, X., Khokiattiwong, S., Kornkanitnan, N., 2019. Sedimentary responses to the sea level and Indian summer monsoon changes in the central Bay of Bengal since 40 ka. Mar. Geol. 415,. https://doi.org/10.1016/j.margeo.2019.05.006 105947.

Licht, A., France-Lanord, C., Reisberg, L., Fontaine, C., Soe, A.N., Jaeger, J.J., 2013. A palaeo Tibete-Myanmar connection? Reconstructing the Late Eocene drainage system of central Myanmar using a multi-proxy approach. J. Geol. Soc. 170, 929–939. https://doi.org/10.1144/jgs2012-126.

Lisiecki, L.E., Raymo, M.E., 2007. Plio-Pleistocene climate evolution: trends and transitions in glacial cycle dynamics. Quat. Sci. Rev. 26, 56–69. https://doi.org/10.1016/j.quascirev.2006.09.005.

Liu, S., Li, J., Zhang, H., Cao, P., Mi, B., Khokiattiwong, S., Kornkanitnan, N., Shi, X., 2020. Complex response of weathering intensity registered in the Andaman Sea sediments to the Indian Summer Monsoon over the last 40 kyr. Mar. Geol. 426,. https://doi.org/10.1016/j.margeo.2020.106206 106206.

Lupker, M., France-Lanord, C., Galy, V., Lavé, J., Kudrass, H.,, 2013. Increasing chemical weathering in the Himalayan system since the Last Glacial Maximum. Earth Planet. Sci. Lett. 365, 243–252. https://doi.org/10.1016/j.epsl.2013.01.038.

Madhupratap, M., Gauns, M., Ramaiah, N., Kumar, S.P., Muraleedharan, P.M., de Sousa, S.N., Sardessai, S., Muraleedharan, U., 2003. Biogeochemistry of the Bay of Bengal: physical, chemical and primary productivity characteristics of the central and western Bay of Bengal during summer monsoon 2001. Deep-Sea Res. II 50, 881–896. https://doi.org/10.1016/S0967-0645(02)00611-2.

Martinson, D.G., Pisias, N.G., Hays, J.D., Imbrie, J., Moore, T.C., Shackleton, N.J., 1987. Age dating and the orbital theory of the ice ages: Development of a high resolution 0 to 300,000 year chronostratigraphy. Quat. Res. 27, 1–29. https://doi.org/10.1016/0033-5894(87)90046-9.

Meehl, G.A., Loschnigg, J., 2003. Coupled Ocean-Atmosphere dynamical processes in the Tropical Indian and Pacific Oceans and the TBO. J. Clim. 16, 2138–2158. https://doi.org/10.1175/2767.1.

Meyer, I., Davies, G.R., Stuut, J.-B.-W., 2011. Grain size control on Sr-Nd isotope provenance studies and impact on paleoclimate reconstrctions: an example from deep-sea sediments offshore NW Africa. Geochem. Geophys. Geosyst. 12, 1–14. https://doi.org/10.1029/2010GC003355.

Meyers, P.A., 1994. Preservation of elemental and isotopic source identification of sedimentary organic matter. Chem. Geol. 114, 289–302. https://doi.org/10.1016/0009-2541(94)90059-0.

Milliman, J.D., Farnsworth, K.L., 2011. Asia. In: River DischArge to the CoAstAl OceAn: A GlobAl Synthesis. Cambridge Univ. Press, New York, pp. 289–311. https://doi.org/10.1017/CBO9780511781247.012.

Miranda, J., Baliarsingh, S., Lotliker, A., Sahoo, S., Sahu, K., Kumar, T., 2020. Long-term trend and environmental determinants of phytoplankton biomass in coastal waters of northwestern Bay of Bengal. Environ. Monit. Assess. 192, 55. https://doi.org/10.1007/s10661-019-8033-8.

Miriyala, P., Sukumaran, N.P., Nath, B.N., Ramamurty, P.B., Sijinkumar, A.V., Vijayagopal, B., Ramaswamy, V., Sebastian, T., 2017. Increased chemical weathering during the deglacial to mid-Holocene summer monsoon intensification. Sci. Rep. 7, 44310. https://doi.org/10.1038/srep44310.

Mohtadi, M., Prange, M., Schefuß, E., Jennerjahn, T.C., 2017. Late Holocene slowdown of the Indian Ocean Walker circulation. Nat. Comm. 8, 1015. https://doi.org/10.1038/s41467-017-00855-3.

Moore, D.M., Reynolds, R.C., 1989. X-ray diffraction and the identification and analysis of clay minerals. Oxford Univ. Press, Oxford, p. 332.
Mortlock, R.A., Froelich, P.N., 1989. A simple method for the rapid determination of biogenic opal in pelagic marine sediments. Deep-Sea Res. A 36, 1415–1426. https://doi.org/10.1016/0198-0149(89)90092-7.
Naidu, A.S., Mowatt, T.C., Somayajulu, B.L.K., Rao, K.S., 1985. Characteristics of Clay Minerals in the Bed Loads of Major Rivers of India. Mitteilungen aus dem Geologische-Palaontologischen Instituts der. Universitat Hamburg 58, 559–568.
Naidu, P.D., Malmgren, B.A., 1999. Quaternary carbonate record from the equatorial Indian Ocean and its relationship with productivity changes. Mar. Geol. 161, 49–62. https://doi.org/10.1016/S0025-3227(99)00055-9.
Narvekar, J., Kumar, S.P., 2014. Mixed layer variability and chlorophyll *a* biomass in the Bay of Bengal. Biogeosciences 11, 3819–3843. https://doi.org/10.5194/bg-11-3819-2014.
Nelson, D.M., Treguer, P., Brzezinski, M.A., Leynaerts, A., Queguiner, B., 1995. Production and dissolution of biogenic silica in the ocean: Revised global estimates, comparison with regional data, and relationship to biogenic sedimentation. Global Biogeochem. Cycles 9, 359–372. https://doi.org/10.1029/95GB01070.
Officer, C., Ryther, J., 1980. The possible importance of silicon in marine eutrophication. Mar. Ecol. Prog. Ser. 3, 83–91. https://doi.org/10.1023/A:1021392618824.
Ota, Y., Kawahata, H., Kuroda, J., Yamaguchi, A., Suzuki, A., Araoka, D., Abe-Ouchi, A., Yamada, Y., Ijiri, A., Kanamatsu, T., 2018. Indian monsoonal variations during the past 80 kyr recorded in NGHP-02 Hole 19B, western Bay of Bengal: implications from chemical and mineral properties. Geochem. Geophys. Geosyst. 20, 148–165. https://doi.org/10.1029/2018GC007772.
Ota, Y., Kuroda, J., Yamaguchi, A., Suzuki, A., Araoka, D., Ishimura, T., Kawahata, H., 2019. Monsoon-influenced variations in plankton community structure and upper-water column stratification in the western Bay of Bengal during the past 80 ky. Palaeogeogr. Palaeoclimatol. Palaeoecol. 521, 138–150. https://doi.org/10.1016/j.palaeo.2019.02.020.
Pang, X., Bassinot, F., Sepulcre, S., 2021. Indonesian Throughflow variability over the last two glacial-interglacial cycles: Evidence from the eastern Indian Ocean. Quat. Sci. Rev. 256, 106839. https://doi.org/10.1016/j.quascirev.2021.106839.
Panmei, C., Naidu, P.D., Naik, S.S., 2018. Variability of terrigenous input to the Bay of Bengal for the last ~80 kyr: Implicaions on the Indian monsoon variability. Geo-Mar. Lett. 38, 341–350. https://doi.org/10.1007/s00367-018-0538-6.
Peketi, A., Mazumdar, A., Pillutla, S.P.K., Sawant, B., Gupta, H., 2021. Glimatic and tectonic control on the Bengal fan sedimentation since the Pliocene e2020GC009448 Geochem. Geophys. Geosys. 22. https://doi.org/10.1029/2020GC009448.
Petrick, B., Martinez-Garcia, A., Auer, G., Reuning, L., Auderset, A., Deik, H., Takayanagi, H., Vleeschouwer, D.D., Iryu, Y., Haug, G.H., 2019. Glacial indonesian throughflow weakening across the mid-pleistoncene climatic transition. Sci. Rep. 9, 16995. https://doi.org/10.1038/s41598-019-53382-0.
Phillips, S.C., Johnson, J.E., Underwood, M.B., Guo, J., Giosan, L., Rose, K., 2014. Long-timescale variation in bulk and clay mineral composition of Indian continental margin sediments in the Bay of Bengal, Arabian Sea, and Andaman Sea. Mar. Pet. Geol. 58, 117–138. https://doi.org/10.1016/j.marpetgeo.2014.06.018.
Prasanna Kumar, S., Muraleedharan, P.M., Prasad, T.G., Gauns, M., Ramaiah, N., Desouza, S.N., Sardesai, S., Madhupratap, M., 2002. Why is the bay of bengal less productive during summer monsoon compared to the Arabian Sea? Geophys. Res. Lett. 29, 2235. https://doi.org/10.1029/2002GL016013.
Prasanna Kumar, S., Nuncio, M., Ramaiah, N., Sardesai, S., Narvekar, J., Fernandes, V., Paul, J.T., 2007. Eddy-mediated biological productivity in the Bay of Bengal during fall and spring intermonsoons. Deep Sea Res. I 54, 1619–1640. https://doi.org/10.1016/j.dsr.2007.06.002.
Rachmayani, R., Prange, M., Schulz, M., 2016. Intra-interglacial climate variability: model simulations of Marine Isotope Stages 1, 5, 11, 13, and 15. Clim. Past 12, 677–695. https://doi.org/10.5194/cp-12-677-2016.
Ragueneau, O., Treguer, P., Leynaert, A., Anderson, R.F., Brzezinski, M.A., DeMaster, D.J., Dugdale, R.C., Dymond, J., Fischer, G., Francois, R., Heinze, C., Maier-Reimer, E., Martin-Jezequel, V., Nelson, D.M., Queguiner, B., 2000. A review of the Si cycle in the modern ocean: recent progress and missing gaps in the application of biogenic opal as a paleoproductivity proxy. Global Planet. Change 26, 317–365. https://doi.org/10.1016/S0921-8181(00)00052-7.
Raman, C.V., Rao, G.K., Reddy, K.S.N., Ramesh, M.V., 1995. Clay mineral distributions in the continental shelf sediments between the Ganges mouths and Madras, east coast of India. Cont. Shelf Res. 15, 1773–1793. https://doi.org/10.1016/0278-4343(94)00093-3.
Ramaswamy, V., Gaye, B., 2006. Regional variations in the fluxes of foraminifera carbonate, coccolithophorid carbonate and biogenic opal in the northern Indian Ocean. Deep Sea Res. I 53, 271–293. https://doi.org/10.1016/j.dsr.2005.11.003.
Reimer, P.J., Bard, E., Bayliss, A., Beck, J.W., Blackwell, P.G., Ramsey, C.B., 2013. IntCal13 and Marine13 Radiocarbon Age Calibration Curves 0–50,000 Years cal BP. Radiocarbon 55, 1869–1887. https://doi.org/10.2458/azu_js_rc.55.16947.
Saraswat, P., Singh, D.P., Lea, D.W., Mackensen, A., Naik, D.K., 2019. Indonesian throughflow controlled the westward extent of the Indo-Pacific Warm Pool during glacial-interglacial intervals. Global Planet. Change 183,. https://doi.org/10.1016/j.gloplacha.2019.103031 103031.
Sarma S.S., V.V., Rao D., G., Viswanadham, R., Sherin K., C., Salisbury, J., Omand, M. M., Mahadevan, A., Murty N., V.S., Shroyer, E.L., Baumgartner, M., Stafford M., K., 2016. Effects of freshwater stratification on nutrients, dissolved oxygen, and phytoplankton in the Bay of Bengal. Oceanography 29, 222–231 https://www.jstor.org/stable/24862685.
Saylor, J.E., Casturi, L., Shanahan, T.M., Nie, J.S., Saadeh, C.M., 2016. Tectonic and climate controls on Neogene environmental change in the Zhada Basin, southwestern Tibetan Plateau. Geology 44, 919–922. https://doi.org/10.1130/G38173.1.
Schneider, N., 1997. The Indonesian throughflow and the global climate systems. J. Clim. 11, 676–689. https://doi.org/10.1175/1520-0442(1998)011<0676:TITATG>2.0.CO;2.
Schott, F.A., McCreary Jr., J.P., 2001. The monsoon circulation of the Indian Ocean. Prog. Oceanogr. 51, 1–123. https://doi.org/10.1016/S0079-6611(01)00083-0.
Sijinkumar, A.V., Nath, B.N., Guptha, M.V.S., 2010. Late Quaternary record of pteropod preservation from the Andaman Sea. Mar. Geol. 275, 221–229. https://doi.org/10.1016/j.margeo.2010.06.003.
Singh, S.K., France-Lanord, C., 2002. Tracing the distribution of erosion in the Brahmaputra watershed from isotopic compositions of stream sediments. Earth Planet. Sci. Lett. 202, 645–662. https://doi.org/10.1016/S0012-821X(02)00822-1.
Singh, A., Gandhi, N., Ramesh, R., 2012. Contribution of atmospheric nitrogen deposition to new production in the nitrogen limited photic zone of the northern Indian Ocean. J. Geophys. Res. (Oceans) 117, C06004. https://doi.org/10.1029/2011JC007737.
Singh, A.D., Jung, S.J., Darling, K., Ganeshram, R., Ivanochko, T., Kroon, D., 2011. Productivity collapses in the Arabian Sea during glacial cold phases 2009PA001923 Paleoceanogr. Paleoclimatol. 26. https://doi.org/10.1029/2009PA001923.
Singh, S.K., Rai, S.K., Krishnaswami, S., 2008. Sr and Nd isotopes in river sediments from the Ganga basin: Sediment provenance and spatial variability in physical erosion. J. Geophys. Res. 113, F03006. https://doi.org/10.1029/2007JF000909.
Spero, H.J., Mielke, K.M., Kalve, E.M., Lea, D.W., Pak, D.K., 2003. Multispecies approach to reconstructing eastern equatorial Pacific thermocline hydrography during the past 360 kyr. Paleoceanogr. Paleoclim. 18, 1022. https://doi.org/10.1029/2002PA000814.
Sprintall, J., Rèvelard, A., 2014. The Indonesian Throughflow response to Indo-Pacific climate variability. J. Geophys. Res. (Oceans) 119, 1161–1175. https://doi.org/10.1002/2013JC009533.
Stokke, P.R., Carson, B., 1973. Variation in clay mineral X-ray diffraction results with the quantity of sample mounted. J. Sediment. Petrol. 43, 957–964.
Storey, M., Roberts, R.G., Saidin, M., 2012. Astronomically calibrated $^{40}Ar/^{39}Ar$ age for the Toba supereruption and global synchronization of late Quaternary records. Proc. Nat. Acad. Sci. 109, 18684–18688. https://doi.org/10.1073/pnas.1208178109.
Stuiver, M., Reimer, P.J., 1993. Extended ^{14}C data base and revised CALIN 3.0 ^{14}C age calibration program. Radiocarbon 35, 215–230. https://doi.org/10.1017/S0033822200013904.
Su, Q., Nie, J., Meng, Q., Heermance, R., Gong, L., Luo, Z., Wang, Z., Zhang, R., Garzione, C., 2019. Central Asian dryin at 3.3 Ma linked to tropical forcing? 2019GL084648 Geophys Res. Lett. 46, 10561–10567. https://doi.org/10.1029/2019GL084648.
Sun, X., Liu, S., Fang, X., Li, J., Cao, P., Zhao, G., Khokiattiwong, S., Kornkanitnan, N., Shi, X., 2020. Clay minerals of surface sediments from the lower Bengal Fan: Implications for provenance identification and transport processes. Geol. J. 55, 6038–6048. https://doi.org/10.1002/gj.3786.
Terray, P., Dominiak, S., Delecluse, P., 2005. Role of the southern Indian Ocean in the trasitions of the monsoon-ENSO system during recent decades. Clim. Dyn. 24, 169–195. https://doi.org/10.1007/s00382-004-0480-3.
Thomson, J.R., Holden, P.B., Anand, P., Edwards, N.R., Porchier, C.A., Harris, N.B.W., 2021. Tectonic and climatic dirvers of Asian monsoon evolution. Nat. Comm. 12, 4022. https://doi.org/10.1038/s41467-021-24244-z.
Tripathi, G.R., Singh, S.K., Bhushan, R., Ramaswamy, V., 2011. Sr-Nd isotope composition of the Bay of Bengal sediments: Impact of climate on erosion in the Himalaya. Geochem. J. 45, 175–186. https://doi.org/10.2343/geochemj.1.0112.
Vuba, S., Ahmad, S.M., Anipindi, N.R., 2015. Geochemical and mineralogical studies in recent clastic sediments from upper Godavari river in peninsular India. J. Geol. Soc. India 86, 107–114. https://doi.org/10.1007/s12594-015-0286-4.
Wang, P.X., Wang, B., Cheng, H., Fasullo, J., Guo, Z.T., Kiefer, T., Liu, Z.Y., 2017. The global monsoon across time scals: Mechanisms and outstanding issues. Earth Sci. Rev. 174, 84–121. https://doi.org/10.1016/j.earscirev.2017.07.006.
Weber, M.E., Lantzsch, H., Dekens, P., Das, S.K., Reilly, B.T., Martos, Y.M., Meyer-Jacob, C., Agrahari, S., Ekblad, A., Titschack, J., Holmes, B., Wolfgramm, P., 2018. 200,000 years of monsoonal history recorded on the lower Bengal Fan - strong response to insolation forcing. Global Planet. Change 166, 107–119. https://doi.org/10.1016/j.gloplacha.2018.04.003.
Webster, P.J., 1987. The Elementary Monsoon. In: Fein, J.S., Stephens, P.L. (Eds.), Monsoons. Wiley, New York, pp. 3–32.
Yamamoto, M., Clemens, S.C., Seki, O., Tsuchiya, Y., Huang, Y., O'ishi, R., Abe-Ouchi, A., 2022. Increased interglacial atmospheric CO_2 levels followed the mid-Pleistocene Transition. Nat. Geosci. 15, 307–313. https://doi.org/10.1038/s41561-022-00918-1.
Yang, J., Liu, Q., Liu, Z., 2010. Linking observations of the Asian monsoon to the Indian Ocean SST: Possible roles of Indian Ocean Baisn mode and Dipole mode. J. Clim. 23, 5889–5902. https://doi.org/10.1175/2010JCLI2962.1.
Yu, Z., Colin, C., Bassinot, F., Wan, S., Bayon, G., 2020. Climate-driven weathering shifts between highlands and floodplains e2020GC008936 Geochem. Geophys. Geosyst. 21. https://doi.org/10.1029/2020GC008936.
Zorzi, C., Goni, M.F.S., Anupama, K., Prasad, S., Hanquiez, V., Johnson, J., Giosan, L., 2015. Indian monsoon variations during three contrasting climatic periods: The Holocene, Heinrich Stadial 2 and the last interglacial-glacial transition. Quat. Sci. Rev. 125, 50–60. https://doi.org/10.1016/j.quascirev.2015.06.009.